Korean J. Chem. Eng., **31**(5), 754-771 (2014)
DOI: 10.1007/s11814-013-0254-x

pISSN: 0256-1115
eISSN: 1975-7220

Power-law shear-thinning flow around a heated square bluff body under aiding buoyancy at low Reynolds numbers

Neha Sharma, Amit Dhiman†, and Surendra Kumar

Department of Chemical Engineering, Indian Institute of Technology Roorkee, Roorkee 247 667, India
(*Received 8 September 2013 • accepted 26 November 2013*)

Abstract−Power-law shear-thinning fluid flow over a heated square bluff body is numerically investigated under aiding buoyancy mixed convection at low Reynolds numbers. Semi-explicit finite volume code is developed to solve the governing equations along with the appropriate boundary conditions. Both aiding buoyancy and shear-thinning natures are found to augment the heat transfer rate from the surface of the long square bar. In aiding buoyancy, the total drag coefficient is found to be more for the square cylinder than that of the circular cylinder, whereas the average cylinder Nusselt number for the square cylinder is found to be lower than the circular one on equal side/diameter basis. Maximum augmentation in heat transfer is found to be approximately 20% with respect to forced convection. Finally, a heat transfer correlation is established by using the Colburn heat transfer factor.

Keywords: Square Bluff Body, Non-Newtonian Fluids, Aiding Buoyancy, Drag Coefficients, Nusselt Number, Streamlines, Isotherms and Heat Transfer Enhancement

INTRODUCTION

Shear-thinning is the property of fluids to reduce their viscosity as the shear force is applied on them, which makes them very useful in many industrial applications, such as in novel heat exchange systems, continuous thermal treatment of food stuffs, polymer processing, chemical, biological, food and mineral process engineering applications and so forth. Under appropriate conditions of flow and heat transfer, multiphase mixtures such as foams, paper pulp suspensions, emulsions, fiber reinforced resin processing, and high molecular weight slurries and polymeric materials like solutions, blends, and melts exhibit shear-thinning behavior. In such settings, the flow behavior depends mainly upon the number of obstacles, type or nature of fluid flow, free stream flow or channel flow, buoyancy effect, blockage ratio, Reynolds number. In the literature, extensive information is now available on the non-Newtonian flow around (horizontal) regular and non-regular obstacles [1-5], but only a few studies exist for the flow around a square cylinder in the vertical configuration, albeit for Newtonian fluids [6-9]. Therefore, it becomes essential to be acquainted with the behavior of non-Newtonian fluids around the cylinder of square cross-section for the upward flow. Thus, we studied momentum and heat transfer phenomena of shear-thinning fluids around the long square obstacle under the influence of aiding buoyancy in the unconfined vertical arrangement. The buoyancy effects when superimposed on the flow strongly influence the flow and thermal patterns and are of particular significance at low velocity and/or when the temperature difference between the body and the ambient fluid is large. The pertinent literature is given below on both Newtonian and non-Newtonian flows under the impact of mixed convection around circular and square bluff bodies.

†To whom correspondence should be addressed.
E-mail: dhimuamit@rediffmail.com, amitdfch@iitr.ac.in

The unconfined Newtonian flow and heat transfer under the buoyancy effects over a square cylinder in both vertical and horizontal configurations have been recently reviewed in [6]. Briefly, Sharma and Eswaran [7] studied the effect of aiding/opposing buoyancy ($-1\le Ri\le 1$) on the flow and heat transfer characteristics around an isolated square cylinder for the fixed Reynolds number (Re) of 100 and the Prandtl number (Pr) of 0.7 (air). Subsequently, they [8] extended their study [7] to investigate the aiding/opposing buoyancy ($-1\le Ri\le 1$) around a square cylinder in a channel for the varying values of blockage ratios (10%-50%) for Re=100 and Pr=0.7. Chatterjee and Mondal [9] examined the influence of aiding/opposing buoyancy around a heated/cooled square cylinder for Re=50-150, $-1\le Ri\le 1$ and Pr=0.7 for two blockage ratios of 2% and 25% by using Fluent. The vortex shedding frequency increases with increased heating and suddenly reduces to zero at the critical Richardson number. On the cross-buoyancy, Bhattacharyya and Mahapatra [10] studied the effect of buoyancy ($0\le Ri\le 1$) on vortex shedding and heat transfer from a square cylinder to air for $Re\le 1400$. Subsequently, Dhiman et al. [11] elucidated the effects of cross-buoyancy on the flow and heat transfer characteristics of an isothermal square cylinder confined in a channel for the fixed blockage ratio of 12.5% ($1\le Re\le 30$, $0.7\le Pr\le 100$ and $0\le Ri\le 1$). Chatterjee and Mondal [12] performed simulations to understand the influence of cross-stream buoyancy on the vortex shedding process behind a stationary heated square cylinder at low Reynolds numbers (Re=5-40, Ri=0-2 and Pr=0.7). On the non-Newtonian fluid flow around the long square obstacle under the influence of cross-buoyancy, as far as we know, only two studies are reported in the open literature [13,14]. Dhiman et al. [13] analyzed the steady laminar mixed convection to Newtonian and power-law fluids from a heated square cylinder for the range of situations as Re=1-30, n=0.8-1.5, Pr=0.7-100 ($Pe\le 3000$) for Richardson number (Ri)=0-0.5. The effects of Prandtl number and of power-law index on the heat transfer are found to be more prominent than that of buoyancy parameter ($Ri\le 0.5$). Bouaziz

et al. [14] predicted numerically the flow and heat transfer of power-law fluids in a plane channel with a built-in heated square cylinder for the constant blockage ratio of 12.5% (n=0.5, 1 and 1.4, Re=20-200, Ri=0-8, Pr=50). They obtained the heat transfer correlations through forced convection. Surprisingly, no information is available on the non-Newtonian momentum and heat transfer around the square cylinder under the impact of aiding/opposing buoyancy.

On the other hand, extensive studies on the non-Newtonian forced convection flow and heat transfer around a square cylinder are reported in the literature. In the unconfined domain, Paliwal et al. [15] explored the two-dimensional (2-D) steady flow of power-law liquids past a square cylinder for Re=5-40, n=0.5-1.4 and Pe=5-400. The lower the value of power-law index, the higher will be the Reynolds number at which a visible wake will appear. Dhiman et al. [16] numerically analyzed the steady flow of power-law fluids over an isolated square cylinder for Re=1-45 and n=0.5-2. The shear-thinning behavior ($n<1$) increases the drag above its Newtonian value ($n=1$), whereas the shear-thickening behavior ($n>1$) reduces the drag below its Newtonian value. Dhiman et al. [17] investigated the heat transfer to power-law fluids from a heated square cylinder for the range of settings: $1\le Re\le 45$, $0.5\le n\le 2$ and $1\le Pr\le 100$ ($Pe\le 4000$). They obtained appropriate predictive correlations for estimating the value of the heat transfer for two classical thermal boundary conditions, namely isothermal and isoflux. Sahu et al. [18] extended the study of Dhiman et al. [17] for the unsteady laminar flow of power-law fluids across a square cylinder for Re=60-160 and n=0.5-2. The leading edge separation in shear-thinning fluids produces an increase in drag values with the increasing Reynolds number, while shear-thickening behavior delays this separation and shows the lowering of the drag with the Reynolds number. Sahu et al. [19] investigated the heat transfer to power-law fluids from a heated square cylinder in the unsteady cross-flow regime (Re=60-160, n=0.5-1.8 and Pr=0.7-50). Broadly, the shear-thinning fluid behavior promotes heat transfer, whereas the shear-thickening behavior impedes it. Rao et al. [20] extended the study of Dhiman et al. [17] for the 2-D flow of power-law fluids over a square cylinder for Re=0.1-40, n=0.2-1.4 and Pr=0.7-100 by using Fluent. They delineated the values of the Reynolds number denoting the onset of flow separation and the limits of the steady flow regime for both shear-thinning and shear-thickening type fluids. The shear-thinning characteristics can augment the rate of heat transfer by up to 100% under appropriate conditions. Similarly, in the confined domain, plenty of information on the forced convection momentum and heat transfer of non-Newtonian power-law fluids around a square cylinder can be found elsewhere [21-24].

It is also appropriate here to briefly recount the non-Newtonian studies around a circular counterpart because the present study deals with shear-thinning fluids, and also we have compared the present square cylinder results with circular one on equal side/diameter basis in this study (section 4). In the unconfined arrangement, Soares et al. [25] looked into the steady flow of power-law fluids across a heated circular cylinder to determine the dependence of individual drag components and of heat transfer characteristics on power-law index ($0.5\le n\le 1.4$), Prandtl number ($1\le Pr\le 100$) and Reynolds number ($5\le Re\le 40$). The effect of power-law index on such flow behavior is strongly conditioned by the kinematic conditions and less so by the type of thermal boundary condition prescribed at the cylinder surface. Soares et al. [26] numerically studied the mixed convection heat transfer characteristics from a cylinder immersed in power-law fluids (n=0.6, 0.8, 1, 1.6) for Re=1-30, Ri=0-3 and Pr=1, 100. The effects of increased mixed convection on heat transfer were generally more significant at lower values of power-law index, and such a decrease in power-law index was found to increase the magnitude of the surface-averaged Nusselt number. Bharti et al. [27] considered the heat transfer to power-law fluids from a heated cylinder in the steady cross-flow regime for the range of situations: $5\le Re\le 40$, $0.6\le n\le 2$ and $1\le Pr\le 1000$. They developed simple correlations as functions of pertinent dimensionless variables. Patnana et al. [28] simulated the unsteady flow of power-law fluids over a cylinder in cross-flow for Re=40-140 and n=0.4-1.8. The drag coefficient increases and the lift coefficient decreases with the increasing value of the power-law index. They [29] further extended their study [28] to include the effect of Prandtl number (1-100) on the heat transfer characteristics. The average Nusselt number increases with an increase in the value of Reynolds number and/or Prandtl number. Srinivas et al. [30] considered the effect of aiding buoyancy over an isothermally heated cylinder immersed in power-law fluids in the steady regime (n=0.2-1.8, Ri=0-2, Re=1-40 and Pr=1-100). The buoyancy effects are stronger in shear-thinning fluids and/or at low Reynolds numbers than that in shear-thickening and/or at high Reynolds numbers. On the other hand, sufficient details on the non-Newtonian power-law fluid flow around a circular cylinder in the confined domain can be found elsewhere [31-34].

Other than the numerical studies discussed, some experimental studies are available on Newtonian fluid flow around a long square bar in an unconfined domain. The experiments on the fluid flow and heat transfer around rectangular cylinders were performed by Igarashi [35] for width to height ratios being 0.33-1.5 at high Reynolds numbers (Re=7500-37500). Heat transfer correlations are provided for each surface of the cylinder with aspect ratios for air as working fluid. The average Nusselt number for the side (top and bottom surfaces) and the rear surfaces is found to vary as $Re^{2/3}$ ($0.33\le$width/height≤ 1.5); however, the overall Nusselt number varies as $Re^{2/3}$ ($0.67\le$width/height≤ 1.5) and as $Re^{0.62}$ (width/height=0.33). Ahmed and Yovanovich [36] analyzed experimentally the forced convection heat transfer from isothermal bodies of different shapes. They developed empirical models for the forced convection heat transfer, which were valid for a wide range of Reynolds numbers $0\le Re\le 10^5$ and Pr=0.71. Saha et al. [37] reported the measurements of two-components of velocity in the wake of a square cylinder using a hot-wire anemometer. The measurements were carried out in a low-speed, low-turbulence wind tunnel for two Reynolds numbers, 8700 and 17625. Both velocity and velocity fluctuations show symmetry about the wake axis. They also confirmed the energy transfer from the mean flow to the streamwise velocity fluctuation in the near wake. Singh et al. [38] experimentally investigated the effect of aiding buoyancy on the wakes of circular and square cylinders at low Reynolds numbers (53-118) and Ri ranging from 0.025 to 0.314. The critical Richardson number increases with Reynolds number, and also the critical Ri for a square cylinder is found close to that of a circular cylinder at comparable Re. Sabiri et al. [39] used micro-electrodes made of platinum to measure the local shear rate on the surface of a cylinder (length-to-diameter ratio of 11-12) exposed to the fully developed laminar flow of power-law fluids in a vertical

pipe, with a wide range of Reynolds numbers 0.16≤Re≤75. They used different fluids for their studies and found that their power law index varied as n=0.83, 0.90 and 1. They observed that the shear rate is maximum at about θ=130° and it tends to be higher in shear-thinning fluids than that in Newtonian fluids otherwise under identical conditions.

In the confined domain, sufficient experimental literature on Newtonian flow and heat transfer phenomena around a square bluff body can be found elsewhere (Davis et al. [40], and Suzuki and Suzuki [41]). On the flow of Newtonian/non-Newtonian fluids past a circular cylinder, Coelho and Pinho [42-44] experimentally studied the flow of shear-thinning fluids in the Reynolds number range Re= 50-9000 by using laser-Doppler anemometry. They delineated the various vortex shedding regimes as a function of Reynolds and elasticity numbers (Coelho and Pinho [42]). The flow characteristics within each of these flow regimes were then analyzed in detail by Coelho and Pinho [43]. Coelho and Pinho [44] also carried out measurements of pressure on the cylinder surface for Newtonian and non-Newtonian fluids, and the values of the pressure drag coefficient, pressure rise coefficient and the wake angle were reported.

Hence, as far as we know, no information is available on the mixed convection of non-Newtonian fluids around a square cylinder in the vertical unbounded laminar flow regime, despite its numerous engineering applications. Accordingly, the aim of the present study is set to investigate the momentum and heat transfer characteristics of non-Newtonian power-law fluids under the impact of aiding buoyancy in the vertical unconfined configuration.

PROBLEM STATEMENT, GOVERNING EQUATIONS AND BOUNDARY CONDITIONS

A schematic of the non-Newtonian upward flow and heat transfer around a long heated square bar in the 2-D unconfined domain is depicted in Fig. 1. The artificial boundaries of the flow domain are considered to make the problem computationally feasible. The incompressible power-law fluid enters the flow domain with a uniform velocity V_∞ and at a temperature T_∞ in the vertical direction, from bottom to top. The stationary square cylinder (of side b) is placed symmetrically between the two parallel vertical boundaries and the long square obstacle is maintained at a constant temperature of T_w^* ($>T_\infty$). The width of the computational domain is L_1= 30b in the *x*-direction and the domain height is L_2=32b in the *y*-direction. The distance from the inlet to the front surface of the square cylinder is H_u=10.5b (i.e., upstream distance) and from the rear surface of the square bar to the outlet is H_d=20.5b (i.e., downstream distance). These distances were chosen after a thorough investigation and the details are given in section 3.2.

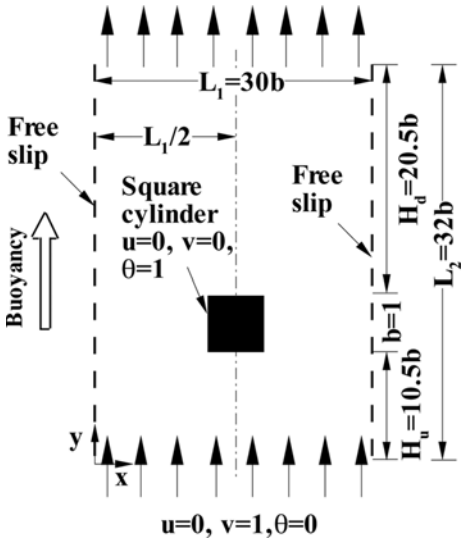

Fig. 1. Schematic of the unconfined flow around a heated square cylinder under the impact of aiding buoyancy.

The thermo-physical properties such as heat capacity and thermal conductivity are assumed to be independent of the temperature, except for the body force term in the momentum equation. The Boussinesq approximation accounts for the thermal buoyancy effects. The viscous dissipation is also assumed to be negligible as Brinkman number is assumed to be small over the range of settings studied here. The 2-D conservative continuity equation (Eq. (1)), *x*- and *y*-components of Cauchy's equations (Eqs. (2) and (3)) and thermal energy equation (Eq. (4)) in their dimensionless form are given as [4,5,45]:

Continuity equation:

$$\frac{\partial u}{\partial x}+\frac{\partial v}{\partial y}=0 \tag{1}$$

x- and *y*-momentum equations:

$$\frac{\partial u}{\partial t}+\frac{\partial (uu)}{\partial x}+\frac{\partial (vu)}{\partial y}=-\frac{\partial p}{\partial x}+\frac{\eta}{Re}\left(\frac{\partial^2 u}{\partial x^2}+\frac{\partial^2 u}{\partial y^2}\right)+\frac{2}{Re}\left(\varepsilon_{xx}\frac{\partial \eta}{\partial x}+\varepsilon_{yx}\frac{\partial \eta}{\partial y}\right) \tag{2}$$

$$\frac{\partial v}{\partial t}+\frac{\partial (uv)}{\partial x}+\frac{\partial (vv)}{\partial y}=-\frac{\partial p}{\partial y}+\frac{\eta}{Re}\left(\frac{\partial^2 v}{\partial x^2}+\frac{\partial^2 v}{\partial y^2}\right)+\frac{2}{Re}\left(\varepsilon_{yy}\frac{\partial \eta}{\partial y}+\varepsilon_{xy}\frac{\partial \eta}{\partial x}\right)+Ri\,\theta \tag{3}$$

Energy equation:

$$\frac{\partial \theta}{\partial t}+\frac{\partial (u\theta)}{\partial x}+\frac{\partial (v\theta)}{\partial y}=\frac{1}{Pe}\left(\frac{\partial^2 \theta}{\partial x^2}+\frac{\partial^2 \theta}{\partial y^2}\right) \tag{4}$$

where the dimensionless parameters are given below:

$$u=\frac{u^*}{V_\infty};\ v=\frac{v^*}{V_\infty};\ x=\frac{x^*}{b};\ y=\frac{y^*}{b};\ t=\frac{t^*}{(b/V_\infty)};\ p=\frac{p^*}{\rho V_\infty^2};\ \theta=\frac{T-T_\infty}{T_w^*-T_\infty};$$

$$Re=\frac{b^n V_\infty^{2-n}\rho}{m};\ Pr=\left(\frac{mc_P}{k}\right)\left(\frac{V_\infty}{b}\right)^{n-1};$$

$$Gr=g\beta_V(T_w^*-T_\infty)b^3\left[\frac{\rho}{m}\left(\frac{V_\infty}{b}\right)^{(1-n)}\right]^2;$$

$$Ri=\frac{Gr}{Re^2}=\frac{g\beta_V(T_w^*-T_\infty)b}{V_\infty^2}\ \text{and}\ Pe=RePr$$

The fluid behavior is represented here by

$$\tau_{ij}=2\eta\varepsilon_{ij}\qquad \text{where (i, j)=(x, y)} \tag{5}$$

and the viscosity (η) of power-law fluids is defined as

$$\eta=\left(\frac{I_2}{2}\right)^{(n-1)/2} \tag{6}$$

where m is the power-law consistency index, n is the power-law index (n<1 and n=1 imply shear-thinning and Newtonian behaviors, respectively) and I_2 is the second invariant of the rate of strain tensor, $I_2/2=2(\partial u/\partial x)^2+2(\partial v/\partial y)^2+(\partial u/\partial y+\partial v/\partial x)^2$.

The physical boundary conditions for the flow system under consideration in their dimensionless form can be written as (Fig. 1): At the inlet boundary: u=0, v=1 and θ=0 (uniform and isothermal flow); on left and right boundaries: u=0, $\partial v/\partial x=0$ and $\partial\theta/\partial x=0$ (slip and adiabatic); on the surface of the long square obstacle: u=0, v=0 and θ=1 (no-slip and uniform temperature), and at the exit boundary: $\partial u/\partial y=0$, $\partial v/\partial y=0$ and $\partial\theta/\partial y=0$ (Neumann condition). In addition, homogeneous Neumann boundary conditions are utilized for the pressure at all boundaries, except at the outlet. Dirichlet boundary condition is implemented at the outlet.

The governing mass, momentum and energy equations (Eqs. (1)-(4)) along with the above noted boundary conditions are used to solve the shear-thinning flow and heat transfer around the square cylinder in terms of velocities u(x, y) and v(x, y), pressure p(x, y) and temperature θ(x, y) fields.

NUMERICAL METHODOLOGY

The identical computational grid structure is found adequate here as used in our recent study [6]. The non-uniform computational grid is generated by writing a code in MATLAB. The grid structure has five separate zones in both *x*- and *y*-directions, and uniform as well as non-uniform grid distributions are utilized in the full computational domain, whereas a half domain is exploited in the steady state regime. The grid distribution is made uniform with a constant cell size (Δ) of 0.25b outside a region around a square cylinder that extends 4b upstream, downstream and sideways. A very fine grid of much smaller size (δ) of 0.01b is clustered around the square cylinder over a distance of 1.5b to capture the wake-wall interactions satisfactorily. A hyperbolic tangent function is utilized for stretching the cell sizes between the limits of δ and Δ [46].

The semi-explicit finite volume code implemented on the collocated grid arrangement is used to solve the governing equations along with the appropriate boundary conditions, in which momentum equations are discretized in an explicit manner and the pressure gradient terms are treated implicitly [6,13,16,45,47]. As a result, the pressure-velocity coupling reduces to a Poisson equation for the pressure correction. The possible oscillations due to pressure-velocity decoupling on the collocated grid have been avoided by using the momentum interpolation scheme of Rhie and Chow [48]. In brief, two steps are implemented at each time level: first, a predictor step, a predicted velocity is obtained from the discretized momentum equation using the previous time-level pressure field; second, the corrector step, consists of iterative solution of the pressure-correction equation and in obtaining the corresponding velocity corrections such that the final velocity field satisfies the continuity equation to the prescribed limit. The convective terms are discretized using the third-order accurate QUICK scheme, though the diffusive and non-Newtonian terms are discretized using the central difference scheme (CDS). The velocity fields obtained by solving the momentum equations are used as input to the energy equation. The explicit scheme has also been used for the solution of the energy equation to obtain the temperature field at the each time level and is used for the solution of velocity field at the next time level. The convective term in the energy equation is discretized by using the QUICK scheme and the diffusive term is discretized by using CDS. Because no information is available in the literature for the transition from steady to time-periodic regime for the flow of non-Newtonian power-law fluids around a square bluff body, the time-periodic calculations were carried out here at the extreme values of Re and n For this, a second-order explicit scheme is used for the time discretization. Also, a dimensionless time step of 0.01 is found adequate, as the smaller value of the time step did not produce any considerable change in the values of physical output parameters considered. The convergence criterion of 10^{-9} is set to the residuals and is found suitable.

As the accuracy of numerical results depends largely on the grid and domain sizes, based upon our own experience and others [6,7, 13,30], the grid size, upstream and downstream distances and width of the computational domain are finalized in this work and the details are presented in subsequent subsections.

1. Grid Dependence Study

The grid resolution study is performed by experimenting with various grid sizes to find the optimum size of the grid to capture the wall interactions of long square bar with the fluid adequately. In particular, this is done by comparing the results generated here at three different grid sizes (374×382 cells, 339×347 cells and 264×272 cells with 125, 100 and 50 control volumes (CVs), respectively). Also, it is apparent that as the grid spacing decreases (or the number of CVs increases), the result tends to become relatively accurate. Accordingly, the optimum grid size is selected in such a way that the present results are in the permissible level of tolerance and also that the time of convergence is optimized. Table 1 shows the difference of results produced with the three grid sizes of 0.008b, 0.01b and 0.02b for the extreme cases of n=0.6 and 1 for Re=40, Pr=50 and Ri=0 and 1. At n=1, the percentage relative deviation (with respect to the results at the highest grid size) for the values of pressure drag, friction drag, overall drag and Nusselt number for the grid size of 0.01b is found to be under 0.6%, 0.5%, 0.6% and 0.2%, respectively; whereas, for the grid size of 0.02b, it is less than 3.2%, 2.4%,

Table 1. Grid dependence study at Re=40 and Pr=50 for n=1 and 0.6 and for Ri=0 and Ri=1

S. No.	Size of CV	Ri	C_{DP}	C_{DF}	C_D	Nu
			n=1			
1.	0.008b		1.5104	0.2453	1.7557	10.9510
2.	0.01b	0	1.5166	0.2465	1.7632	10.9516
3.	0.02b		1.5585	0.2511	1.8096	11.1200
1.	0.008b		2.0900	0.4902	2.5803	12.0386
2.	0.01b	1	2.1028	0.4924	2.5952	12.0667
3.	0.02b		2.1455	0.4967	2.6422	12.3283
			n=0.6			
1.	0.008b		1.3786	0.1075	1.4930	11.7235
2.	0.01b	0	1.3583	0.1110	1.4693	11.4672
3.	0.02b		1.3995	0.0996	1.4991	11.2971
1.	0.008b		1.9083	0.2999	2.2082	13.8710
2.	0.01b	1	1.9370	0.2901	2.2271	13.7610
3.	0.02b		1.9409	0.2856	2.2265	13.7689

3.1% and 2.4%, respectively, for all the values of Ri scrutinized. However, at n=0.6, the respective deviation of results for the grid size of 0.01b is less than 1.5%, 3.3%, 1.6% and 2.2%, respectively; whereas, for the grid size of 0.02b, it is less than 1.8, 7.4%, 1.0% and 3.7%, respectively, for the values of Ri. Therefore, the grid size of 339×347 cells is found appropriate to generate further results in the present study.

2. Domain Dependence Study

As the domain dependence study is very essential in numerical investigations it is generally divided into three elements: upstream independence, downstream independence and computational width independence tests. Analogous to the grid dependence study, the optimum domain size is selected taking into account the less time of convergence and the acceptable level of tolerance in the converged solution. In the present study, these investigations are performed for the extreme values of n=1 and 0.6, Re=1 and 40, Ri=0 and 1 at Pr=50.

The upstream independence test is accomplished for upstream distances of 10.5b (339×347) and 12.5b (339×355), while the downstream distance and the width of the domain are kept constant as 20.5b and 30b, respectively. For Newtonian fluids (n=1), the rela-

Table 2. Validation for Newtonian and non-Newtonian flows in a lid-driven square cavity at Re=100 for varying values of power-law index (n)

Source	u_{min}	v_{max}	v_{min}
n=0.75			
Sahu et al. [20]	−0.2386	0.2260	−0.2657
Present work	−0.2368	0.2265	−0.2657
n=1			
Ghia et al. [48]	−0.2109	0.1753	−0.2453
Present work	−0.2107	0.1752	−0.2468
n=1.5			
Sahu et al. [20]	−0.1811	0.1408	−0.2236
Present work	−0.1821	0.1400	−0.2226

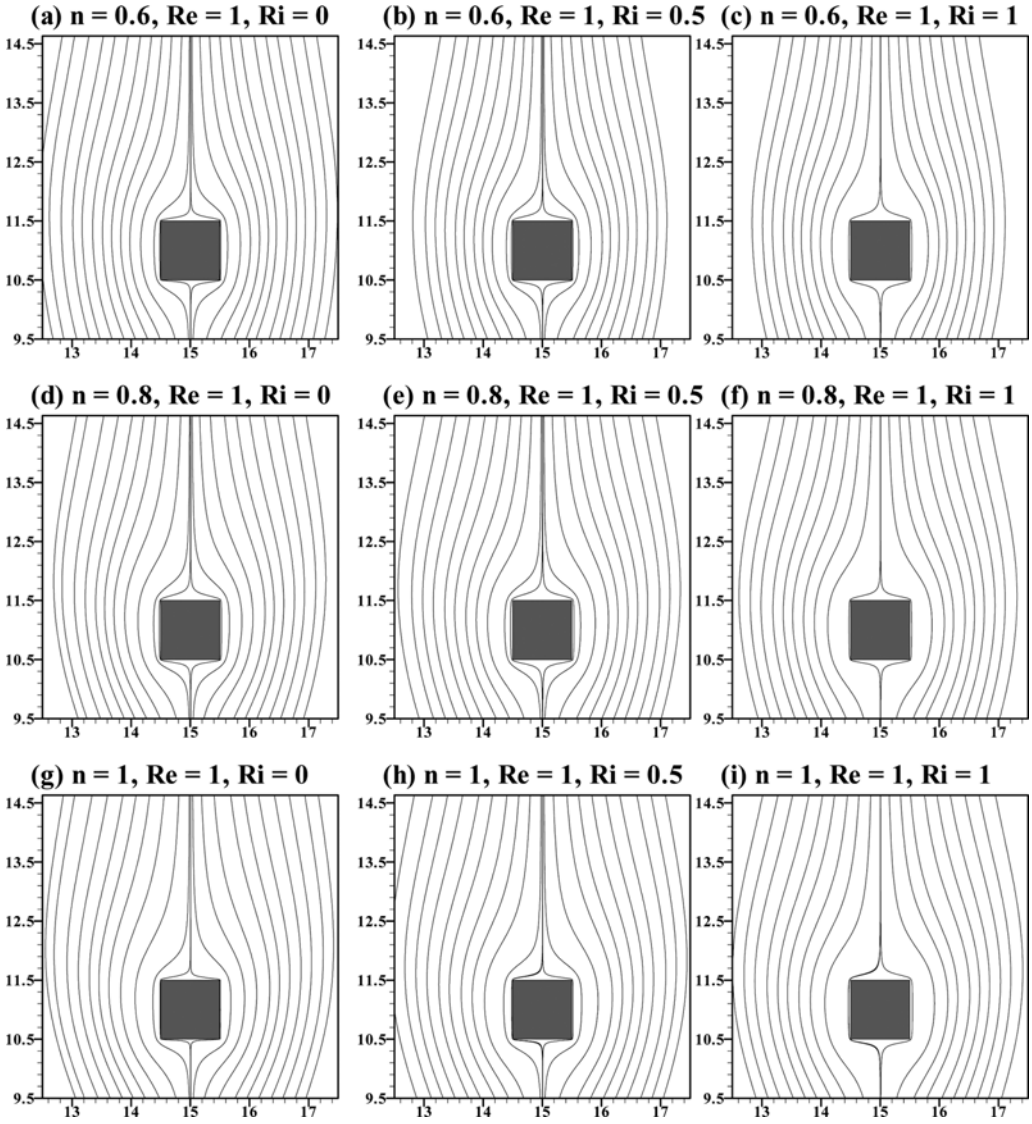

Fig. 2. Streamline contours around the square cylinder at Re=1 for n=0.6-1 and Ri=0-1.

tive difference in the values of pressure drag, friction drag, overall drag and Nusselt number is found to be less than 0.2%, 2.1%, 0.6%, 0.4% (for Re=1 and Ri=0); 0.9%, 0.5%, 0.8%, 1.4% (for Re=40 and Ri=0); 0.9%, 1.8%, 0.02%, 0.4% (for Re=1 and Ri=1) and 0.5%, 0.1%, 0.4%, 0.1% (for Re=40 and Ri=1), respectively. The test is also performed for the non-Newtonian behavior (n=0.6) at various physical parameters, and the results of C_{DP}, C_{DF}, C_D and Nu obtained are under 3.9%, 3.2%, 3.7%, 4.5% (for Re=1 and Ri=0); 0.9%, 2.2%, 1.0%, 1.0% (for Re=40 and Ri=0); 2.3%, 1.9%, 1.6%, 1.1% (for Re=1 and Ri=1) and 1.8%, 2.7%, 1.2%, 0.4% (for Re=40 and Ri=1), respectively. Hence, the dimensionless upstream distance of 10.5 is used in this study.

Likewise, the downstream dependence study is carried out for the distances of 16.5b (339×331) and 20.5b (339×347) with the upstream distance of 10.5b and the width of the domain of 30b. For Newtonian fluids (n=1) the percentage difference in the values of pressure drag, friction drag, overall drag and Nusselt number is less than 4.7%, 1.0%, 3.4%, 0.1% (for Re=1 and Ri=0); 0.1%, 1.1%, 0.2%, 1.4% (for Re=40 and Ri=0); 0.2%, 0.1%, 0.1%, 0.007% (for Re=1 and Ri=1) and 0.002%, 0.02%, 0.002%, 0.01% (for Re=40 and Ri=1), respectively. When the analysis is performed for the non-Newtonian fluids (n=0.6), then the percentage deviation is below 1.5%, 3.1%, 2.0%, 3.7% (Re=1 and Ri=0); 1.4%. 4.6%, 1.0%, 2.3% (Re=40 and Ri=0); 4.0%, 4.4%, 4.1%, 4.6% (Re=1 and Ri=1) and 0.8%, 0.2%, 0.7%, 0.4% (Re=40 and Ri=1), respectively. Thus, the dimensionless downstream distance of 20.5 is found adequate for the range of settings considered.

In the same way, subsequent to upstream and downstream dependence studies, the width of the computational domain is experimented for 20b (299×347) and 30b (339×347). And, the study is executed for the extreme values of n=1 and 0.6, Re=1 and 40, Ri=0 and 1 at Pr=50. The relative differences in the values of pressure drag, friction drag, overall drag and Nusselt number for Newtonian fluids (n=1) are found less than 4.2%, 3.4%, 3.9%, 1.8% (for Re=1 and Ri=0); 2.3%, 1.8%, 2.2%, 0.7% (for Re=40 and Ri=0); 3.9%, 2.7%, 3.5%, 0.9% (for Re=1 and Ri=1) and 0.5%, 0.2%, 0.4%,

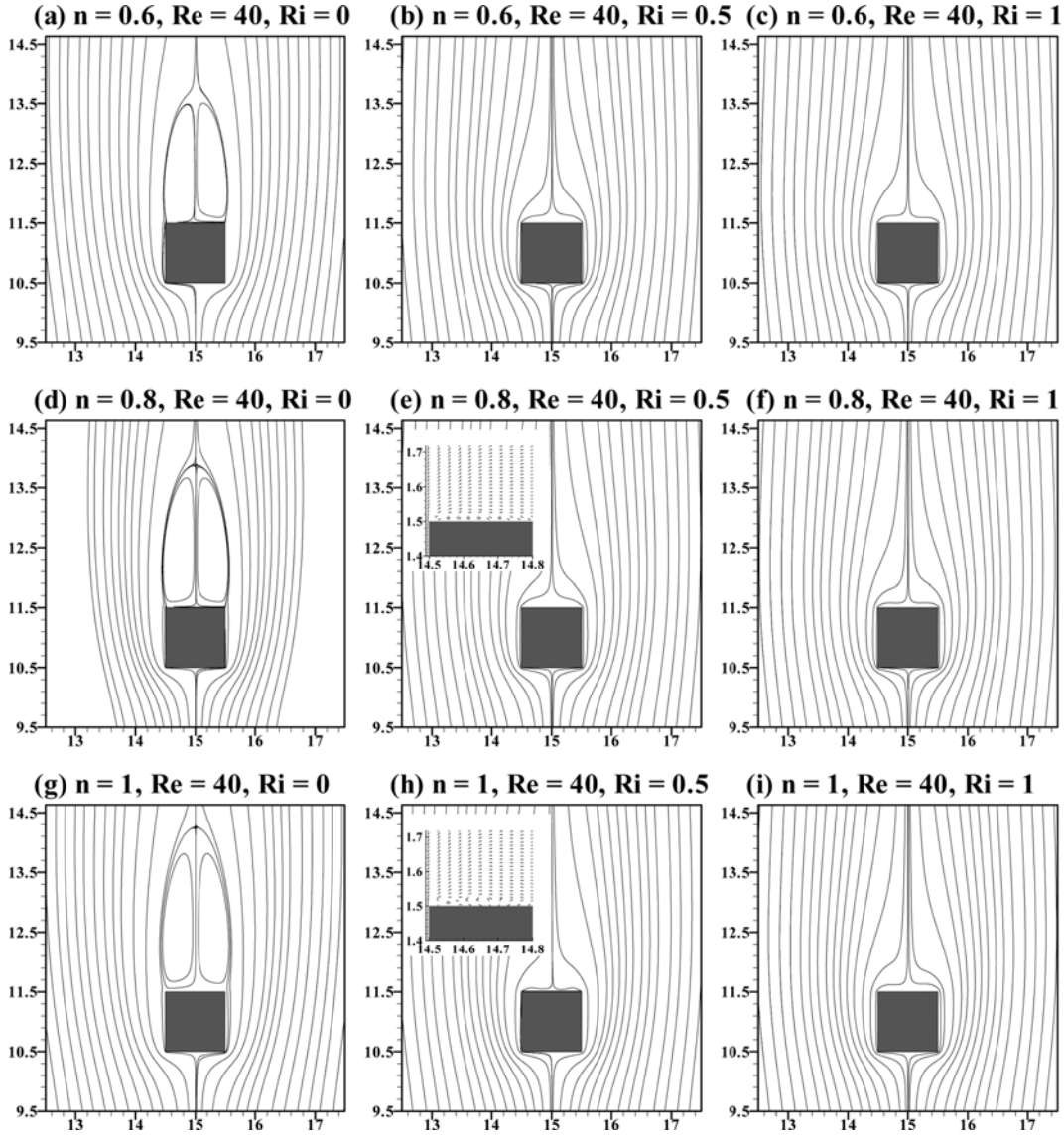

Fig. 3. Streamline contours around the square cylinder at Re=40 for n=0.6-1 and Ri=0-1.

0.1% (for Re=40 and Ri=1), respectively. Whereas, for the non-Newtonian fluids of power-law index n=0.6, the corresponding percentage difference is below 1.7%, 0.1%, 1.2%, 3.8% (for Re=1 and Ri=0); 3.5%, 1.5%, 3.2%, 1.3% (for Re=40 and Ri=0); 3.1%, 2.4%, 2.9%, 4.2% (for Re=1 and Ri=1) and 0.6%, 1.0%, 0.4%, 0.6% (for Re=40 and Ri=1), respectively. As a result, the dimensionless width of the computational domain of 30 is utilized for the determination of new results.

RESULTS AND DISCUSSION

This section considers the buoyancy aided mixed convection flow and heat transfer over the long square bar (long in neutral direction) in the vertical unbounded domain for Reynolds number (Re)= 1-40 and buoyancy parameter (Ri)=0-1. Because the difficulty in obtaining the convergence is found with the decreasing value of the power-law index (i.e., n<0.6) due to the highly non-linear nature of the governing equations for shear-thinning fluids [16], the present investigations are limited to 0.6≤n≤1. The heat transfer study is carried out at a Prandtl number (Pr) of 50. The value of the Prandtl number of the order of 50 or so is very common in chemical, petroleum and oil related engineering applications and chosen based on the studies reported elsewhere [5,14,19]. However, before discussing the details of momentum and heat transfer characteristics around the square cylinder, it is customary to validate the current solution methodology with reliable and accurate literature values.

Extensive benchmarking of the present solution procedure for Newtonian fluid flow and heat transfer around the long square cylinder under the impacts of aiding buoyancy and cross-buoyancy can be found in [6] and [49], respectively. Also, no information is available in the open literature for non-Newtonian fluids around a square cylinder in the vertical configuration. Besides, the general validity of the in-house finite volume code is made with Ghia et al. [50] and Sahu et al. [18] for Newtonian and non-Newtonian flows in a lid-driven square cavity, respectively (Table 2). Table 2 illustrates the comparison between the minimum u (u_{min}) and the minimum v (v_{min})

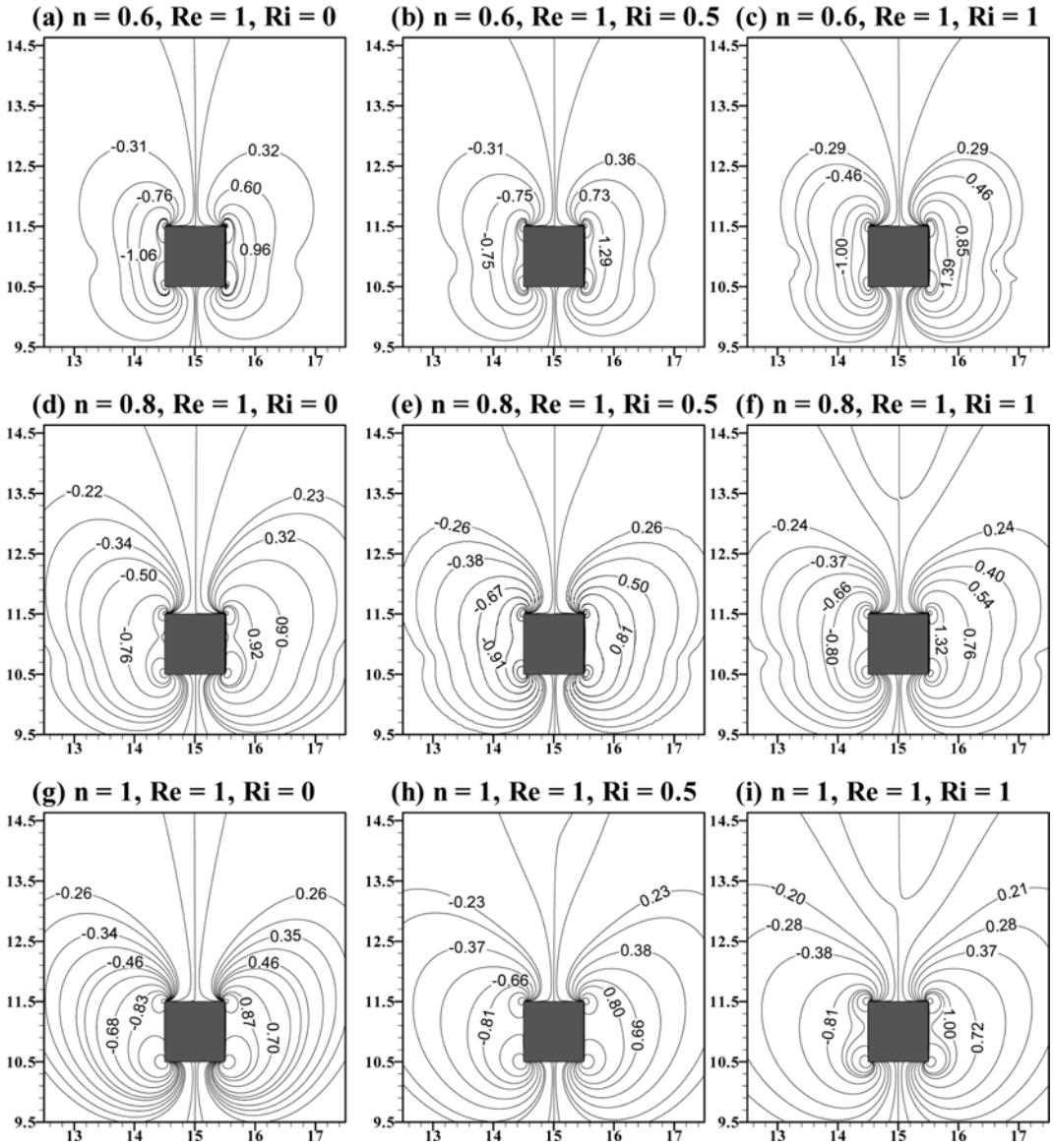

Fig. 4. Vorticity contours around the square cylinder at Re=1 for n=0.6-1 and Ri=0-1.

velocities and the maximum v velocity (v_{max}) at Re=100 for different values of power-law index. The maximum percentage deviation between the velocities for n=0.75, 1 and 1.5 is about 0.5%, 0.01% and 0.7%, respectively. This validates the present numerical methodology.

1. Flow Patterns

In this study, the flow is found to be steady for the range of settings embraced here. Figs. 2(a)-2(i) and 3(a)-3(i) show the streamline contours for Re=1 and 40; n=0.6-1; and Ri=0-1. At Re=1, fluid flow does not separate from the surface of the long square cylinder at different values of Ri and n, as displayed in Figs. 2(a)-2(i). Similarly, for Re>1 at Ri=1 (for n≤1), there is still no wake formation downstream of the square cylinder (Figs. 3(c), 3(f) and 3(i), for instance). While for Newtonian fluids (n=1) at Ri=0, wakes form on the rear surface of the square cylinder for Re≥5 (Fig. 3(g)). However, for Ri=0.5 at n=1, no wake formation is observed for Re<30, but the development of two tiny wakes near the rear corners of the rear surface is found for Re≥30 (Fig. 3(h)). Analogous to Newtonian fluids, for non-Newtonian fluids (n=0.8) at Ri=0, the wakes are observed for Re≥5 (Fig. 3(d)); whereas at Ri=0.5, the appearance of tiny wakes is delayed further to Re=40 (Fig. 3(e)). Figs. 3(e) and 3(h) also include the vector profiles to show the occurrence of two tiny wakes near the rear corners of the rear surface. On the other hand, for n=0.6 at Ri=0, wake formation takes place for Re≥10 (Fig. 3(a), for instance), but when the buoyancy influences the flow (Ri>0), no wake formation is observed (Figs. 3(b) and 3(c)). Thus, it is clear that the wake formation is delayed as the value of power-law index decreases (or with the increasing shear-thinning tendency), while the downstream wakes behind the square cylinder are diminishing with the increasing aiding buoyancy (Ri). This is probably because as buoyancy (Ri) increases, the velocity gradient at the cylinder surface increases and results in reducing the pressure over the surface of the obstacle (as also discussed by Dhiman et al. [51]) and carries momentum components inward towards the surface of the square cylinder, which delays the separation of the streamline and this delayed separation results in a smaller wake. Furthermore, extensive details to delineate the critical value of

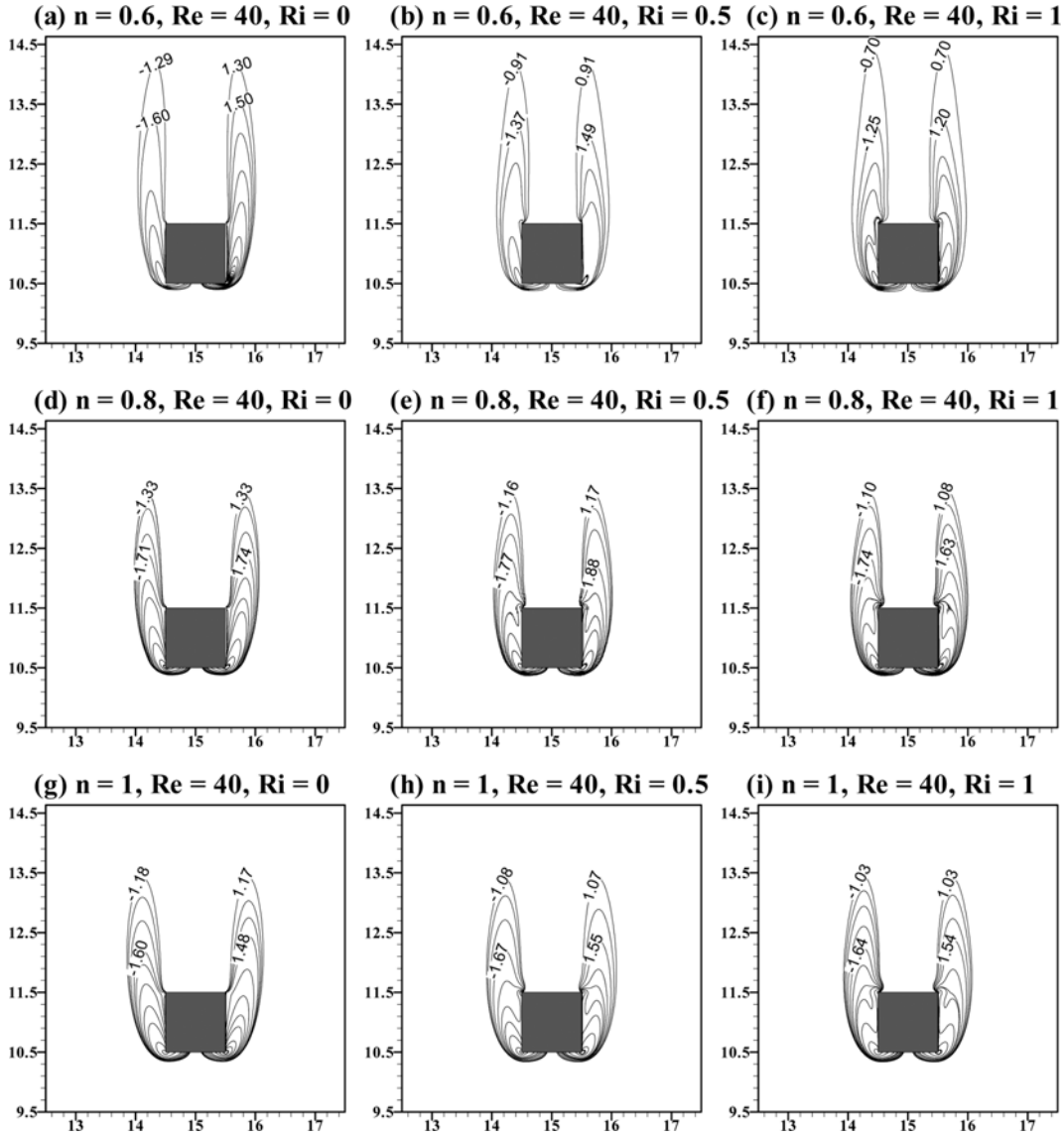

Fig. 5. Vorticity contours around the square cylinder at Re=40 for n=0.6-1 and Ri=0-1.

Ri for the onset of vortex shedding for Newtonian fluids are reported by Gandikota et al. [52], Chatterjee [53] and Chatterjee and Mondal [54].

Also, as the power-law index decreases, the size of the wake also decreases, keeping other parameters constant. The wake size is measured here from the rear surface of the long square obstacle to the point of attachment for the near closed streamline on the centerline. Under the impact of aiding buoyancy (at Ri=0.5), no wake region is observed for any value of n for Re≤20; whereas, two tiny wakes appear at the rear corners of the rear surface of the square

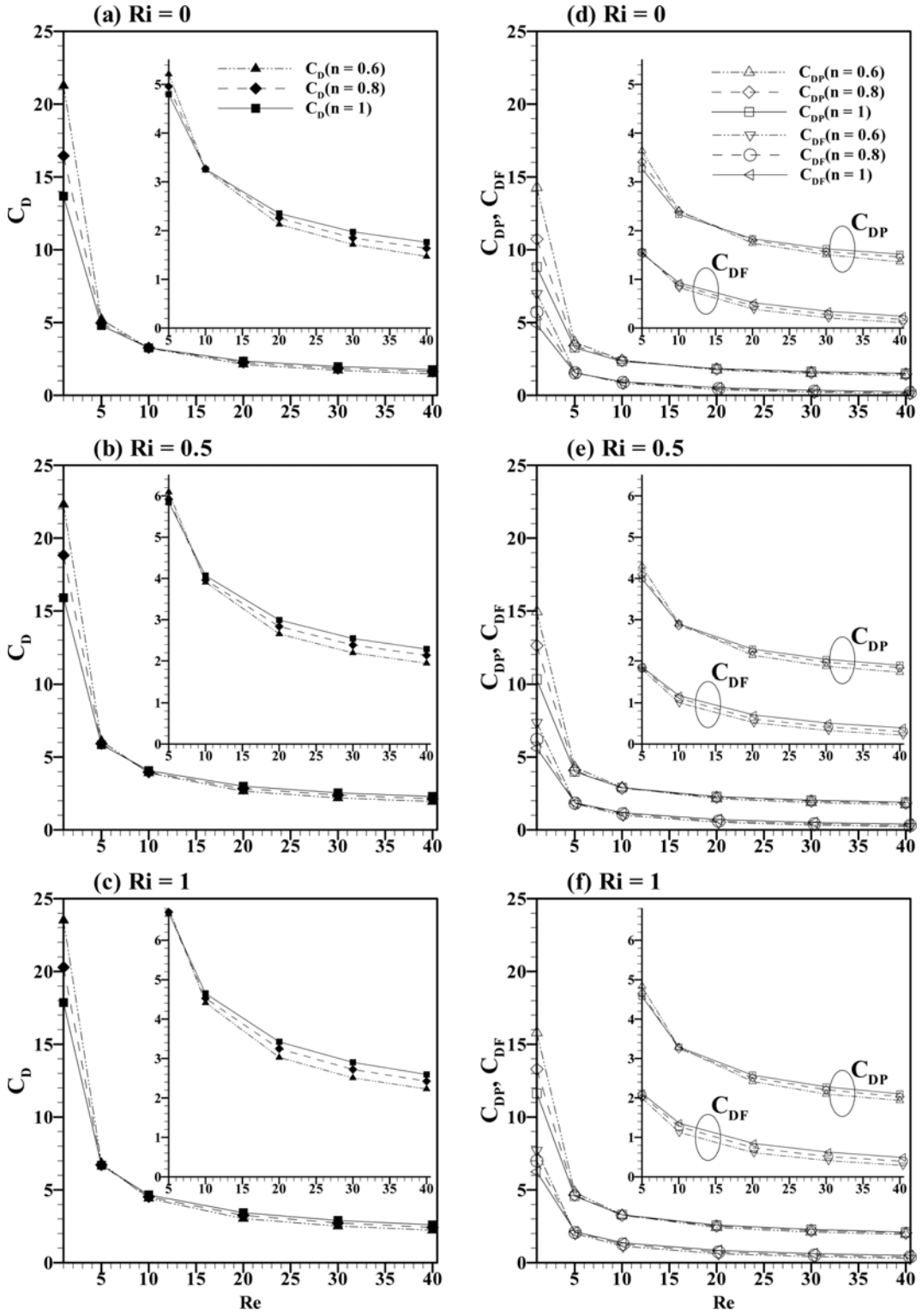

Fig. 6. Friction drag (C_{DF}), pressure drag (C_{DP}) and total drag (C_D) coefficients against Reynolds number (Re) at different values of n and Ri.

cylinder for Re=30 and 40 (at n=1) (Fig. 3(h), for instance) and for Re=40 (at n=0.8) (Fig. 3(e)). Whereas, no such wakes are observed at Ri=1 for the considered range of parameters. Therefore, as the shear-thinning behavior increases, the aiding buoyancy effects are observed to be prominent at higher Reynolds number.

With the help of iso-vorticity contours, the points on the surface of the square cylinder which tends the fluid particles to rotate can be captured. The vorticity contours are illustrated here for Re=1 and 40 at different values of n and Ri in Figs. 4(a)-4(i) and 5(a)-5(i). Also, as Reynolds number and/or power-law index increase(s), the width of the contours decreases; whereas, as the Richardson number increases, the width of the vorticity contours increases. Therefore, one can observe the counter effects of (Re and/or n), and Ri on the width of vorticity contours.

2. Drag Coefficients

The drag coefficient is a dimensionless quantity used to quantify the drag or the resistance of an object in a fluid environment. The drag coefficient is always associated with a particular surface and consists of two basic contributors such as friction drag (or skin drag, C_{DF}) and pressure drag (or form drag, C_{DP}). Therefore, the total drag coefficient (C_D) is mathematically represented as $C_D=C_{DP}+C_{DF}$. Figs. 6(a)-6(f) show the plots of friction drag, pressure drag and total drag coefficients against Reynolds number for different values of power-law index and Richardson number. As expected, the values of individual and overall drag coefficients decrease with the increase in Reynolds number, keeping n and Ri fixed. As the impact of aiding buoyancy increases (from Ri=0-1), the individual and overall drag coefficients increase for the values of n and Re. With the decreasing pseudo-plasticity (or with the increasing value of power-law index) the value of C_D decreases for Re≤5 (for Ri≥0); whereas, for Re>5 (for Ri>0), an opposite trend is observed in the values of C_D with the increasing n. Similarly, for Re>5 (at Ri=0), C_D increases with the increasing n, but at Re=10 a mixed trend is observed with having small differences in the drag values. Similar patterns are also

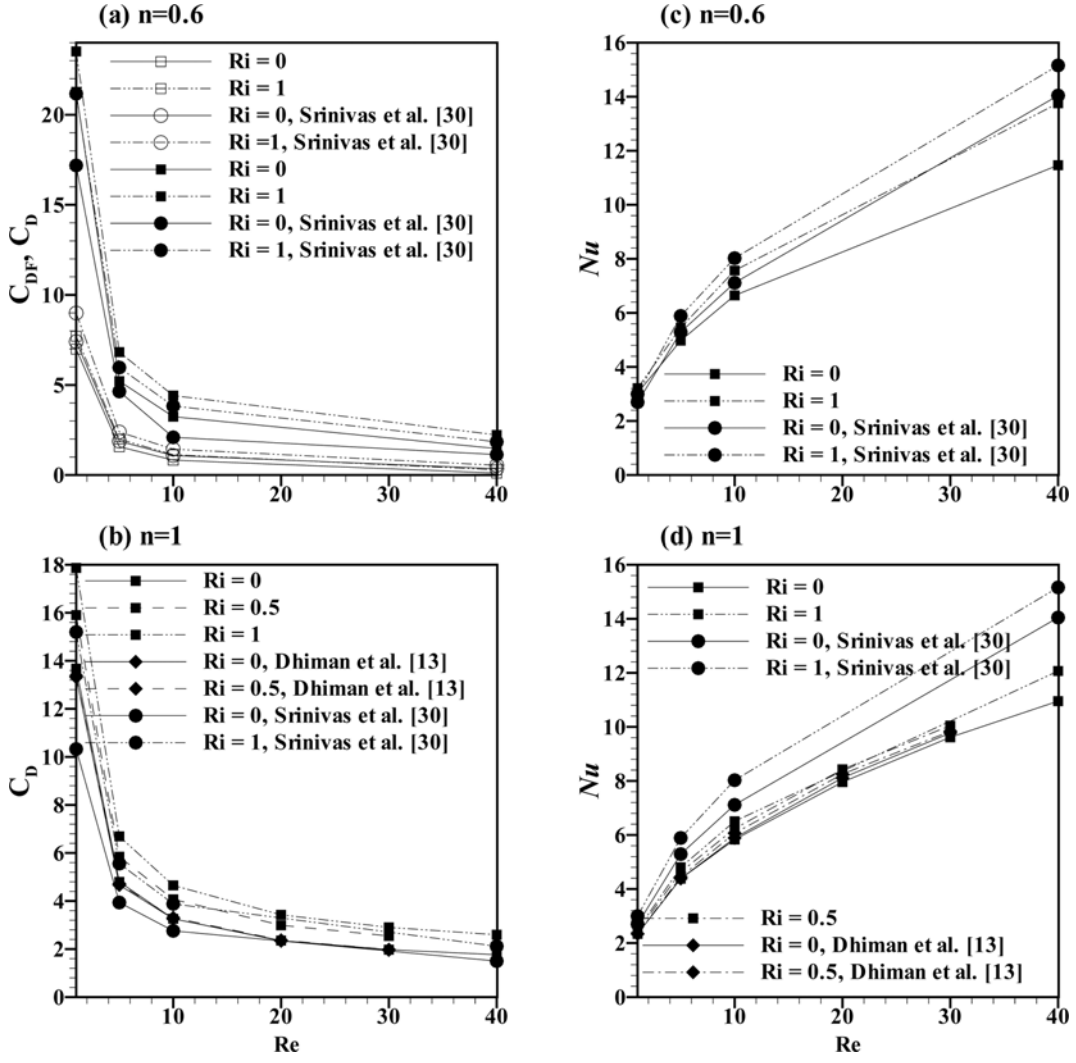

Fig. 7. (a) Shows the comparison of present C_{DF} and C_D at n=0.6 with the results of circular cylinder [30] in the vertical configuration (unfilled and filled symbols correspond to C_{DF} and C_D, respectively), (b) presents the comparison of present C_D at n=1 with circular [30] and square [13] cylinders in vertical and horizontal domains, respectively. Similarly, (c) shows the comparison of present Nu at n=0.6 with the results of circular cylinder [30] in the vertical configuration, (d) presents the comparison of present Nu at n=1 with circular [30] and square [13] cylinders in vertical and horizontal domains, respectively.

seen for pressure drag and friction drag coefficients. Where, the value of C_{DP} decreases for Re≤10 (at Ri=0) and for Re<10 (for Ri>0) as the value of power-law index increases. Along the same line, the value of C_{DP} is found to increase with the power-law index for Re≥ 20 (at Ri≥0). A crossover in the value of pressure drag occurs at Ri=0 between Re=10 and 20; whereas, for Ri>0 (at Re=10) there is seen to be a mixed trend of C_{DP} with very small differences in the values. In the same vein, the C_{DF} values subside for Re=1 (for Ri≥0) and for Re≥10 (for Ri≥0) C_{DF} values increase when the values of power-law index are incremented from 0.6-1. While at Re=5, the value of C_{DF} is observed to decrease at Ri=0 and it increases for Ri>0 with the increasing n with having small value differences. Clearly, when the aiding buoyancy is increased from Ri=0-1, the values of C_{DF}, C_{DP} and C_D are found to increase for all values of Re and n considered [6,7]. These trends are also consistent as documented elsewhere [13] under the influence of cross-buoyancy in the unconfined domain. Likewise, the contribution of the pressure drag to the total drag is always greater than the friction drag (Fig. 6). Broadly, as Ri increases, the thermal buoyancy increases and results in the increase in the pressure gradient, which in turn increases the drag coefficient. For non-Newtonian fluids, as the viscosity of the fluid decreases, the shear forces between fluids and cylinder surfaces decrease, and also the velocity of the fluid increases, which will decrease the boundary layer and thus the pressure gradient is increased. Therefore, the variation in drag coefficient is the combined effect of friction on the surface of the cylinder and the pressure difference.

Further in this section, the relative changes in the values of C_{DF}, C_{DP} and C_D for the effects of aiding buoyancy are observed with respect to Ri=0. The relative difference with Ri is found to be higher at higher values of Re and/or lower values of n (or as the shear-thinning tendency increases). Also, drag coefficients (C_{DF}, C_{DP} and C_D) show a notable change in their values with the increasing value of Ri. For instance, the maximum percentage changes are found about 161.3%, 42.6% and 51.6% (for Re=40, n=0.6 and Ri=1) for the values of C_{DF}, C_{DP} and C_D, respectively, for the whole range of physical parameters studied in this work.

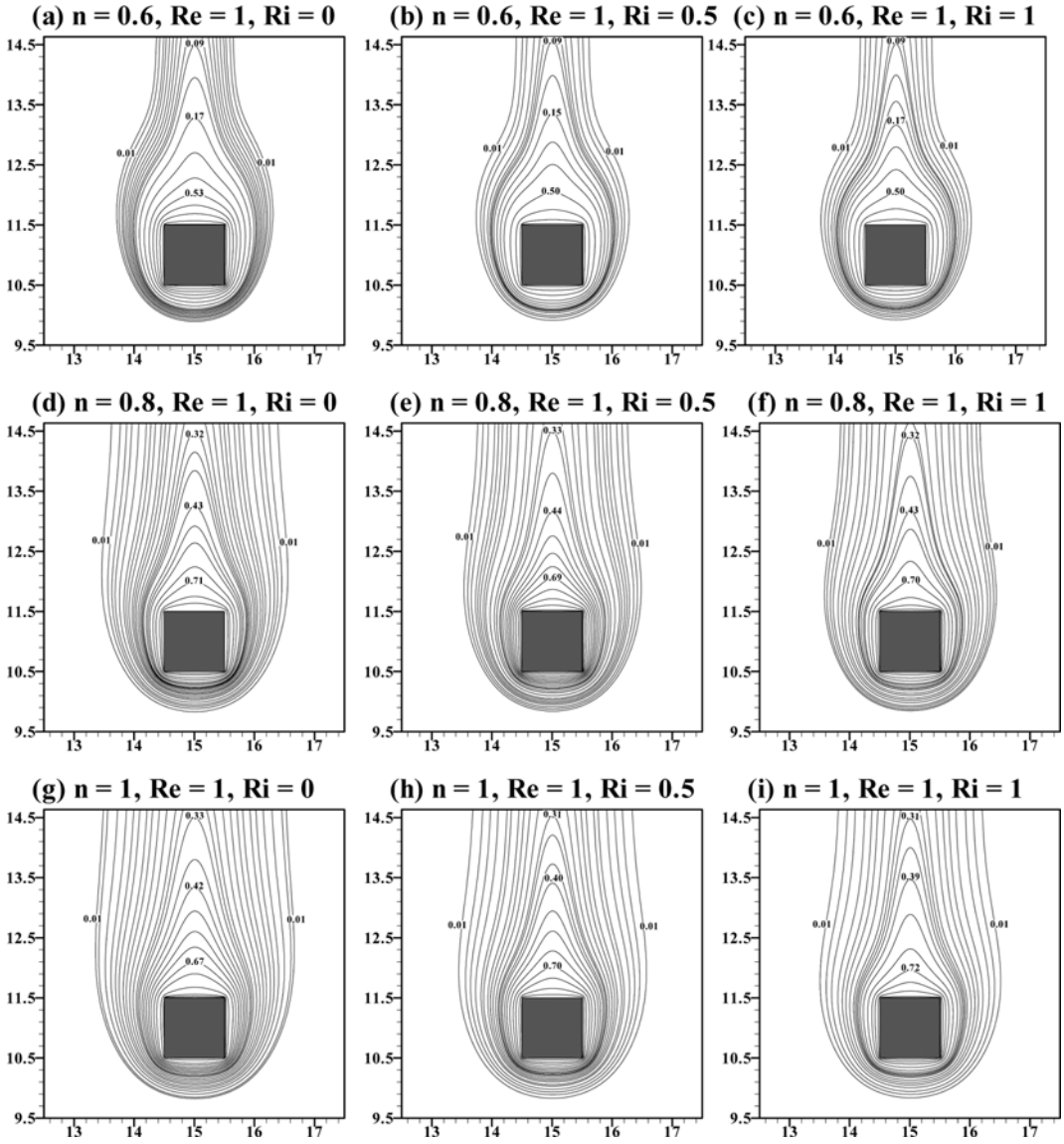

Fig. 8. Isotherm contours around the square cylinder at Re=1 for n=0.6-1 and Ri=0-1.

To represent the estimate of aiding buoyancy and the cross-buoyancy, a comparison of present drag results (around the long square cylinder under the impact of aiding buoyancy in the vertical configuration) is made with the results of Dhiman et al. [13] (around the square cylinder under the effect of cross-buoyancy in the horizontal configuration) and of Srinivas et al. [30] (around the circular cylinder under the aiding buoyancy in the vertical configuration) on equal side/diameter basis at different values of Re, Ri and n in Figs. 7(a)-7(b). It is clear from Fig. 7(a) that for shear-thinning fluids (n=0.6) the present friction drag, C_{DF} (unfilled square symbol) for the square cylinder is less than that of the circular cylinder [30] (unfilled circular symbol) for Ri=0 and 1; whereas, the present total drag coefficient (filled square symbol) is always greater than that of the circular one [30] (filled circular symbol) at different values of Ri. Similarly, for the Newtonian case (n=1), the present C_D (filled square symbol) for the square cylinder is found to be more than the values of C_D for circular one [30] (filled circular symbol) for Ri=0 and 1 (Fig. 7(b)). This can be explained on the basis of the difference in the separation mechanisms for circular and square obstacles. For instance, hydrodynamic instability is more intensified due to sharp corners of a square cylinder as compared to a regular circular cylinder. Also, a stronger buoyancy force is needed for suppression in the case of a square cylinder. Alike, the present value of the total drag coefficient (filled square symbol) under aiding buoyancy is always greater than that of C_D in the cross-buoyancy [13] (filled diamond symbol) for Ri=0 and 0.5 (Fig. 7(b)). This is because under aiding buoyancy the inertial force is combined with the viscous force, and hence, reduces the hydrodynamic instability.

3. Thermal Patterns

Isotherm contours are plotted for the extreme values of Re (1 and 40) in Figs. 8(a)-8(i) and 9(a)-9(i) at different values of Ri and n. As the Reynolds number is increased the lateral width of the isotherm contours (in the downstream) decreases for the fixed Ri and n. This is because at lower values of Reynolds number the heat transfer is predominantly through conduction, but as the Reynolds number increases, convection starts playing a major role [6,12]. The clus-

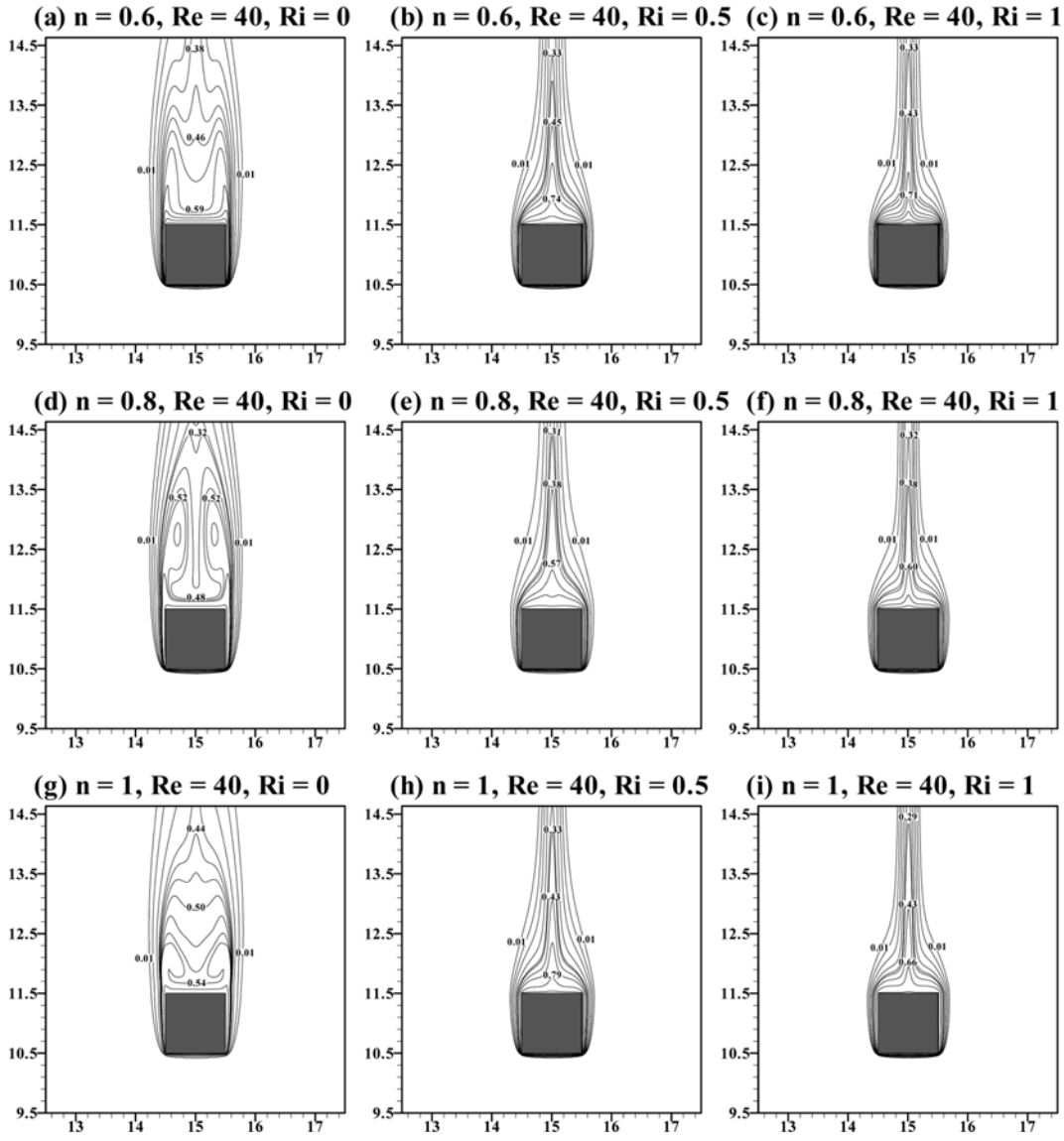

Fig. 9. Isotherm contours around the square cylinder at Re=40 for n=0.6-1 and Ri=0-1.

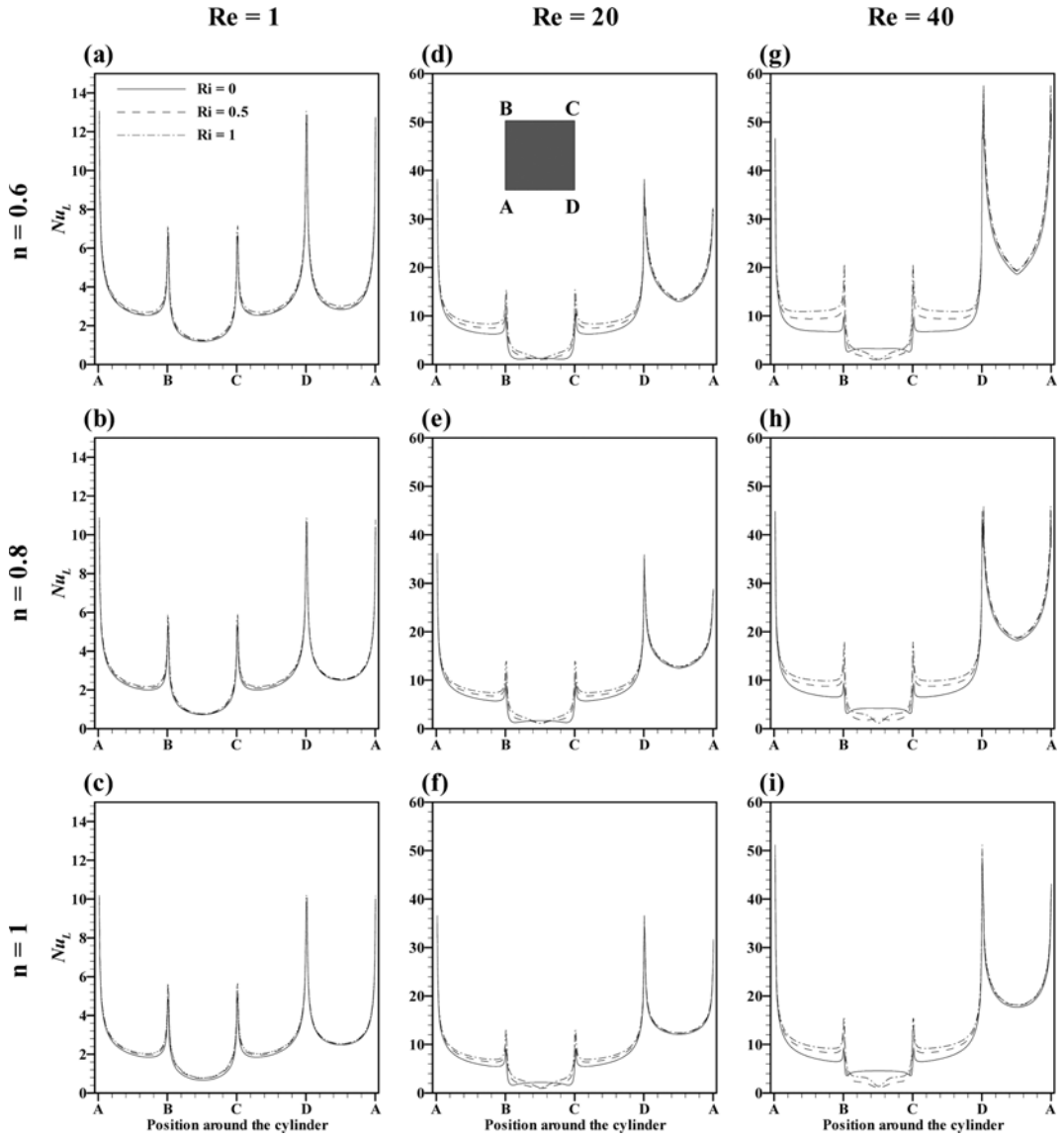

Fig. 10. Variation of the local Nusselt number on the four surfaces of 2-D square cylinder for Re=1, 20 and 40 at different values of n and Ri.

tering of isotherms around the long square obstacle is observed to increase with Re for the constant values of Ri and n, and hence the rate of heat transfer increases with the increase in Reynolds number.

Analogous to the isotherm behavior observed for the Reynolds number, the lateral width of the contours also decreases with the increasing aiding buoyancy (Ri). This causes a thinning of the thermal boundary layer, which accentuates the increase in heat transfer rate, keeping other parameters constant. Also, with the increasing aiding buoyancy the clustering of the isothermal contours around the cylinder surfaces increases and the buoyancy effects are observed to be more prominent at higher values of Reynolds number and/or with the decreasing value of power-law index.

In the same way, as the power-law index decreases (or shear-thinning tendency increases) the lateral width of the isotherm contours decreases, which leads to an increase in the heat transfer. Therefore, as the shear-thinning tendency of fluid increases, the crowding of the isothermal contours on the upstream surface of the square cylinder increases. The front surface of the square cylinder also has more congestion of isotherms as compared to other surfaces of the square cylinder. Therefore, the heat transfer rate from the front surface of the square cylinder is the maximum and the lowest is from the rear surface of the cylinder.

4. Local and Average Nusselt Numbers

Figs. 10(a)-10(i) show the variation of the local Nusselt number on the four surfaces of the 2-D square cylinder at different values of Re, n and Ri. The local Nusselt number (Nu_L) is defined here as $-\partial\theta/\partial n_s$, where θ is the dimensionless temperature and n_s is the direction normal to the square cylinder surfaces. The variation of the local Nusselt number is found to be symmteric about the centerline as the flow is steady for the range of settings studied. Similar to the horizontal flow configuration, the highest heat transfer takes place from the front surface (AD) of the square cylinder for the upward flow; whereas, the lowest rate of heat is transferred from the rear surface (BC) of the square cylinder and the intermediate from left/right surface (AB/CD). Also, the sharpening of curves for the values of local Nusselt number on the front surface of the square cylinder

are observed with the increasing Re and decreasing n. As expected, the local value of the Nusselt number increases with the increasing value of Re for the constant values of Ri and n. Broadly, the rate of heat tranfer increases with the aiding buoyancy, i.e., as Ri increases the local Nusselt number increases from each surface of the square cylinder. But, on the rear surface of the square cylinder for Re>1, a mixed trend in the values of local Nusselt number is observed with Ri. Also, the turning of isotherms towards the center of the rear surface at Ri=0 can be seen with increasing Re [17]. This is because two downstream symmetric wakes are formed at Ri=0; whereas, with increasing Ri these wakes died out. The value of the local Nusselt number increases with the decrease in the power-law index; therefore, as the shear-thinning tendency increases, the rate of heat transfer increases.

Furthermore, the average Nusselt numbers on each surface of the square cylinder are calculated at various values of Re, Ri and n. Figs. 11(a)-11(d) and 12(a)-12(d) present the variation of the average Nusselt number on front, rear and two side surfaces of the 2-D square cylinder with Re and Ri for n=0.6 and n=1, respectively. Clearly, the average Nusselt number is the maximum for the front surface and the lowest for the rear surface, while the intermediate value of the average Nusselt number is found for left and right surfaces (or side surfaces) of the square cylinder. The average Nusselt number on each surface of the square cylinder increases with the increase in Re and/or Ri for all values of n considered. But, on the rear surface, the average Nusselt number is higher at Ri=0 than the corresponding average Nusselt number for n=0.6 (at Ri=0.5) and for n=1 (at Ri>0) for Re=30 and 40 (Figs. 11(b) and 12(b)). This is due to the two standing symmetric wakes behind the square cylinder for Ri=0, while no such wakes are observed for Ri>0. With the decreasing value of power-law index, the average Nusselt number increases on each surface of the square cylinder.

Further insights are provided by comparing the present Newtonian values of the average Nusselt number on each surface of the square cylinder under the aiding buoyancy with the corresponding available literature values in cross-buoyancy [13]. Figs. 12(a)-12(d) illustrate that the average Nusselt number on all the surfaces (except the rear surface) of the square cylinder is found to be more under the aiding buoyancy than that of cross-buoyancy for the values available in the literature (Re=1-30 and Ri=0-0.5), as can be seen in Figs.

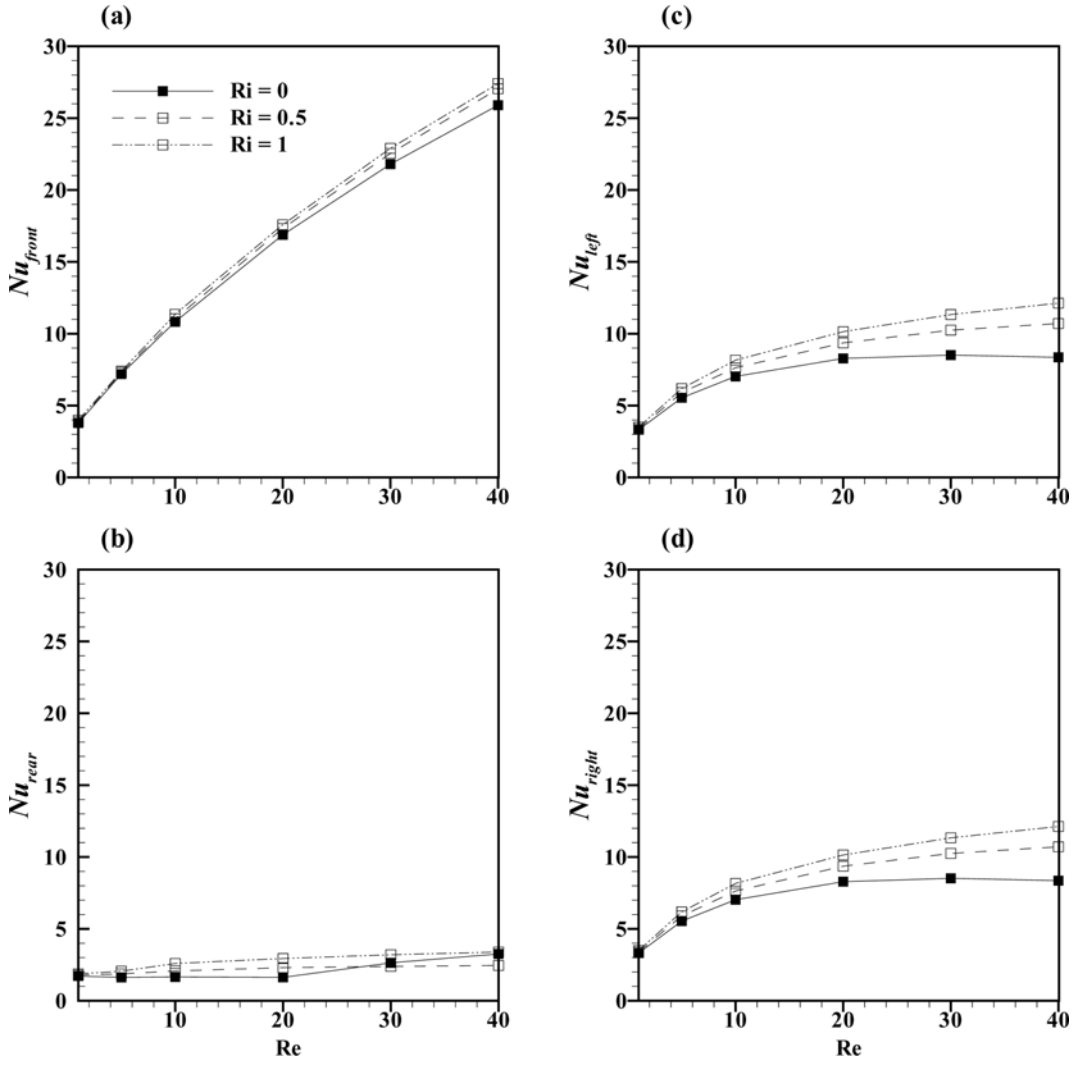

Fig. 11. (a)-(d) Variation of the average Nusselt number on each surface of the square cylinder for n=0.6 at different values of Re and Ri. Filled symbols represent the forced convection fluid flow, while the the hollow symbols represent the buoyancy aided flow.

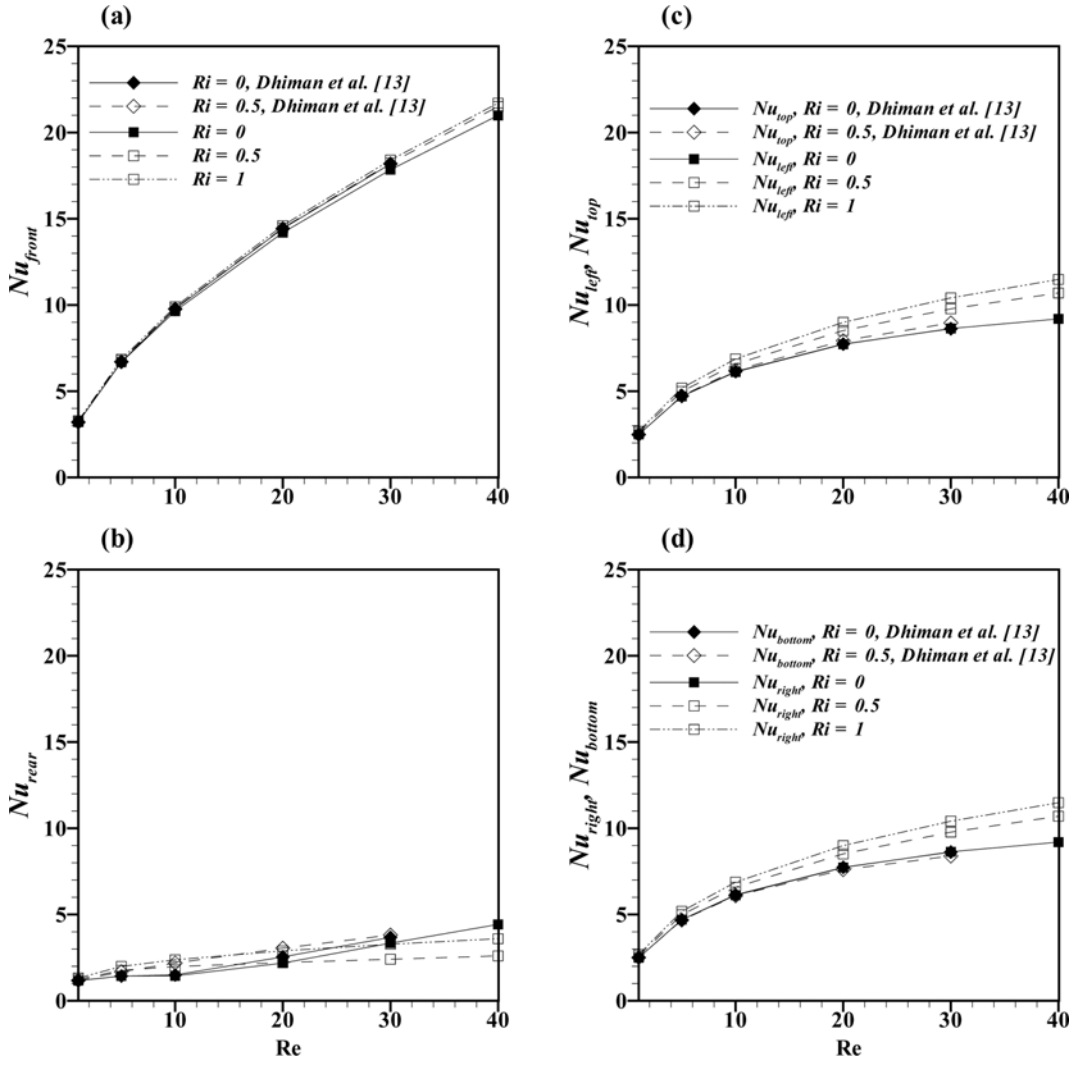

Fig. 12. (a)-(d) Variation of the average Nusselt number (at n=1) on each surface of the square cylinder in horizontal [13] and vertical (present) flow configurations. Identical symbols are used in Figs. (a) and (b).

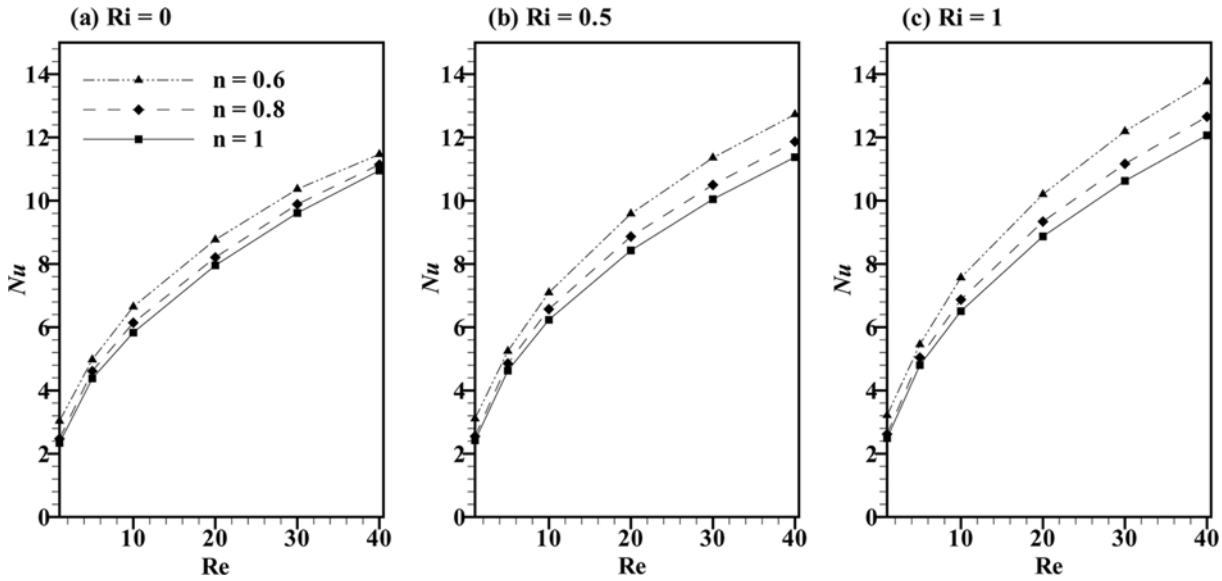

Fig. 13. Average cylinder Nusselt number against Reynolds number at different values of Ri and n.

12(a), 12(c) and 12(d)). Whereas, on the rear surface (Fig. 12(b)), the reciprocal effects are replicated. Particularly, this is due to the different nature of flow strutures downstream of the square cylinder under the effects of aiding buoyancy and cross-buoyancy.

Figs. 13(a)-13(c) show that the average Nusselt number of the square cylinder (Nu) increases with the increase in Reynolds number and/or Richardson number (or aiding buoyancy) for the range of settings considered. Similarly, the average cylinder Nusselt number increases with the decreasing value of the power-law index (or with the increasing shear-thinning behavior). The relative increase in the value of the average cylinder Nusselt number (Nu) increases with Re and/or Ri for the constant value of n. While, with the power-law index, the relative corresponding change in the average cylinder Nusselt number increases at Re = 1 (for Ri>0), and it decreases with the increasing power-law index for Re≥20 (at Ri=0.5) and for Re≥10 (at Ri=1) with respect to Ri=0. However, a mixed trend is noticed for the remaining range of values considered; for instance, at Re=5 the average Nusselt number first decreases from n=0.6-0.8 and then it increases up to n=1 for the values of Ri (=0.5 and 1). And, at Re=10 (for Ri=0.5) the opposite trend is observed, where the relative change first increases and then decreases. The maximum enhancement in the value of the average cylinder Nusselt number (Nu) is about 20% for Re=40, n=0.6 and Ri=1 with respect to Ri=0.

Next, the comparison of the present average cylinder Nusselt number (Nu) for the aiding buoyancy around the square cylinder with the literature values [13,30] for the cross-buoyancy around the square cylinder [13] and for the aiding buoyancy around the circular cylinder [30] is illustrated in Figs. 7(c)-7(d) at different values of Re, Ri and n. From Fig. 7(c), it is clear that at n=0.6 the average cylinder Nusselt number obtained for the fluid flow around the circular cylinder [30] is more than that for the square cylinder (present aiding buoyancy results) for Ri=0 and 1 at all values of Re. Along the same line, the average cylinder Nusselt number for the Newtonian flow (n=1) around the circular cylinder [30] is greater than that for the square cylinder (present aiding buoyancy results) for Re=1-40, Ri=0 and 1 (Fig. 7(d)). Fig. 7(d) also includes the values of the average cylinder Nusselt number for the Newtonian flow around the square cylinder under the impact of cross-buoyancy in the horizontal domain [13]. The present value of the average cylinder Nusselt number under the aiding buoyancy is always greater than that of the corresponding value of the average cylinder Nusselt number in the cross-buoyancy [13] for Ri=0 and 0.5 (Fig. 7(d)). While, the slight difference in the values of the average cylinder Nusselt number at Ri=0 for the square cylinder in both horizontal and vertical domains is due to different domain and grid sizes used [55].

Finally, to correlate the values of the average cylinder Nusselt number (Nu) at various values of Re, Ri and n, the Colburn heat transfer factor 'j_h' is calculated (Eq. (7)), which presumes the validity of $Pr^{1/3}$ assumption.

$$j_h = \frac{Nu}{Re\ Pr^{1/3}} \tag{7}$$

Similar to the study of Dhiman et al. [17], the following simple correlation is developed to correlate the present values of the Colburn heat transfer factor at different values of Re, Ri and n:

$$j_h = 0.635 Re^{-a} n^{-0.14} \tag{8}$$

where the values of constant 'a' are 0.59, 0.57 and 0.543 for Ri=0, 0.5 and 1, respectively. The maximum relative percentage deviation of the above correlation with the present computed results is less than 3.4%, 5.0% and 4.9% for Ri=0, 0.5 and 1, respectively, for all the values of Re and n encompassed here. But, the corresponding maximum deviation for Re=1 could be up to about 17.5% (at Ri=0); 19.5% (at Ri=0.5); 22.0% (at Ri=1) for n=0.6 because of the highly non-linear behavior of the shear-thinning fluids, as well as at low Re the heat transfer is mainly through conduction.

CONCLUSIONS

The combined free and forced convection of non-Newtonian power-law fluid flow and heat transfer around the long heated square bar (long in neutral direction) under the impact of aiding buoyancy are investigated at low Reynolds numbers. Some of the major findings are as follows:

- With the influence of aiding buoyancy, the drag coefficients and the average cylinder Nusselt number are found to increase.
- Under the effect of aiding buoyancy, the total drag coefficient is found to be more for the square cylinder than that of the circular cylinder, whereas the average cylinder Nusselt number for the square cylinder is found to be lower than the circular one on equal side/diameter basis.
- If compared with cross-buoyancy, both the drag coefficient and the average cylinder Nusselt number are always greater in aiding buoyancy.
- The average Nusselt number on each surface of the square cylinder is greater in aiding buoyancy than that of cross-buoyancy, whereas the opposite trend is found for the rear surface of the 2-D square cylinder.
- Heat transfer correlation is obtained for the range of conditions studied.
- Maximum enhancement in the value of the average cylinder Nusselt number is approximately 20% with respect to Ri=0.

NOMENCLATURE

b : side of a square bluff body [m]
c_p : constant pressure specific heat of the fluid [J/kg·K]
C_{DF} : friction drag coefficient ($=2F_{DF}/\rho V_\infty^2 b$)
C_{DP} : pressure drag coefficient ($=2F_{DP}/\rho V_\infty^2 b$)
C_D : total drag coefficient ($=2F_D/\rho V_\infty^2 b=C_{DF}+C_{DP}$)
CV : control volume
F_D : drag force per unit length of the cylinder [N/m]
F_{DF} : frictional force per unit length of the cylinder [N/m]
F_{DP} : pressure force per unit length of the cylinder [N/m]
g : acceleration due to gravity [m/s^2]
Gr : grashof number ($=g\beta_f(T_w^*-T_\infty)b^3[\rho/m(V_\infty/b)^{(1-n)}]^2$)
h : local convective heat transfer coefficient [W/m^2·K]
$\bar{h}$: average convective heat transfer coefficient [W/m^2·K]
H_d : downstream distance [m]
H_u : upstream distance [m]
I_2 : second invariant of the rate of strain tensor, ($=I_2^*/(V_\infty/b)^2$)
j_h : the Colburn heat transfer factor (Eq. (7))
k : thermal conductivity of the fluid [W/m·K]
L_1 : width of computational domain in the x-direction [m]

L_2 : height of the computational domain in the y-direction [m]
m : power-law consistency index [Pa s^n]
n : power-law index [-]
n_s : cylinder surface normal direction [-]
Nu_{bottom} : average Nusselt number on the bottom face of the horizontal cylinder [-]
Nu_{front} : average Nusselt number on the front face of the cylinder [-]
Nu_{left} : average Nusselt number on the left face of the vertical cylinder [-]
Nu_L : local Nusselt number ($=hb/k=-(\partial\theta/\partial n_s|_w)$)
Nu_{rear} : average Nusselt number on the rear face of the cylinder [-]
Nu_{right} : average Nusselt number on the right face of the vertical cylinder [-]
Nu_{top} : average Nusselt number on the top face of the horizontal cylinder [-]
Nu : average cylinder Nusselt number ($=\bar{h}b/k$)
p : pressure ($=p^*/(\rho V_\infty^2)$)
Pe : Peclet number (RePr)
Pr : Prandtl number ($=(mc_P/k)(V_\infty/b)^{n-1}$)
Re : Reynolds number ($=b^n V_\infty^{2-n}\rho/m$)
Ri : Richardson number ($=Gr/Re^2$)
t : time ($=t^*/(b/V_\infty)$)
T : temperature [K]
T_∞ : temperature of the fluid at the inlet [K]
T_w^* : temperature of the surface of the square cylinder [K]
u : component of velocity in the x-direction ($=u^*/V_\infty$)
v : component of velocity in the y-direction ($=v^*/V_\infty$)
V_∞ : uniform velocity of fluid at the inlet [m/s]
x : transverse coordinate ($=x^*/b$)
y : streamwise coordinate ($=y^*/b$)

Greek Symbols

β_V : coefficient of volumetric expansion [1/K]
θ : temperature ($=(T-T_\infty)/(T_w^*-T_\infty)$)
δ : smallest cell size [-]
Δ : largest cell size [-]
ε : rate of deformation tensor, ($=\varepsilon^*/(V_\infty/b)$)
η : power-law viscosity, ($=\eta^*/\eta_0$)
η_0 : reference viscosity, ($=m(V_\infty/b)^{n-1}$) [Pa s]
ρ : density of the fluid at temperature T [kg/m^3]
ρ_0 : density of the fluid at temperature T_∞ [kg/m^3]
τ : extra stress components, ($=\tau^*/(\eta_0 V_\infty/b)$)

Subscripts

∞ : inlet condition
w : surface of the cylinder

Superscript

* : dimensional variable

REFERENCES

1. R. P. Chhabra, *Hydrodynamics of non-spherical particles in non-Newtonian fluids*, In: Cheremisinoff, N. P., Cheremisinoff, P. N. (Eds.), *Handbook of Applied Polymer Processing Technology*, Marcel Dekker, NY, USA (Chapter 1) (1996).
2. R. P. Chhabra, *Heat and mass transfer in rheologically complex systems*, In: Siginer, D., De Kee, D., Chhabra, R. P. (Eds.), *Advances in the Rheology and Flow of Non-Newtonian Fluids*, Amsterdam (Chapter 39) (1999).
3. R. K. Gupta, *Polymer and composites rheology*, second Ed., Marcel Dekker, New York (2000).
4. R. P. Chhabra, *Bubbles, drops, and particles in non-newtonian fluids*, second Ed., CRC Press, Boca Raton, FL (2006).
5. R. P. Chhabra and J. F. Richardson, *Non-newtonian flow and applied rheology*, 2nd Ed., Butterworth-Heinemann, Oxford (2008).
6. N. Sharma, A. K. Dhiman and S. Kumar, *Int. J. Heat Mass Transfer*, **55**, 2601 (2012).
7. A. Sharma and V. Eswaran, *Num. Heat Transfer. A*, **45**, 601 (2004).
8 A. Sharma and V. Eswaran, *Int. J. Heat Mass Transfer.*, **48**, 5310 (2005).
9. D. Chatterjee and B. Mondal, *Heat Transfer. Eng.*, **33**, 1063 (2012).
10. S. Bhattacharyya and S. Mahapatra, *Heat Mass Transfer.*, **41**, 824 (2005).
11. A. K. Dhiman, R. P. Chhabra and V. Eswaran, *Int. Comm. Heat Mass Transfer.*, **35**, 47 (2008).
12. D. Chatterjee and B. Mondal, *Int. J. Heat Mass Transfer.*, **54**, 5262 (2011).
13. A. K. Dhiman, N. Anjaiah, R. P. Chhabra and V. Eswaran, *J. Fluids Eng.*, **129**, 506 (2007).
14. M. Bouaziz, S. Kessentini and S. Turki, *Int. J. Heat Mass Transfer.*, **53**, 5420 (2010).
15. B. Paliwal, A. Sharma, R. P. Chhabra and V. Eswaran, *Chem. Eng. Sci.*, **58**, 5315 (2003).
16. A. K. Dhiman, R. P. Chhabra and V. Eswaran, *Chem. Eng. Res. Des.*, **84**, 300 (2006).
17. A. K. Dhiman, R. P. Chhabra and V. Eswaran, *Num. Heat Transfer. A*, **52**, 185 (2007).
18. A. K. Sahu, R. P. Chhabra and V. Eswaran, *J. Non-Newtonian Fluid Mech.*, **160**, 157 (2009).
19. A. K. Sahu, R. P. Chhabra and V. Eswaran, *Num. Heat Transfer. A*, **56**, 109 (2009).
20. P. K. Rao, A. K. Sahu and R. P. Chhabra, *Int. J. Heat Mass Transfer.*, **54**, 390 (2011).
21. A. K. Gupta, A. Sharma, R. P. Chhabra and V. Eswaran, *Ind. Eng. Chem. Res.*, **42**, 5674 (2003).
22. A. K. Dhiman, *Int. J. Therm. Sci.*, **48**, 1552 (2009).
23. A. K. Sahu, R. P. Chhabra and V. Eswaran, *Num. Heat Transfer. A*, **58**, 641 (2010).
24. A. K. Sahu, R. P. Chhabra and V. Eswaran, *J. Non-Newtonian Fluid Mech.*, **165**, 752 (2010).
25. A. A. Soares, J. M. Ferreira and R. P. Chhabra, *Ind. Eng. Chem. Res.*, **44**, 5815 (2005).
26. A. A. Soares, J. Anacleto, L. Caramelo, J. M. Ferreira and R. P. Chhabra, *Ind. Eng. Chem. Res.*, **48**, 8219 (2009).
27. R. P. Bharti, R. P. Chhabra and V. Eswaran, *Int. J. Heat Mass Transfer*, **50**, 977 (2007).
28. V. K. Patnana, R. P. Bharti and R. P. Chhabra, *Chem. Eng. Sci.*, **64**, 2978 (2009).
29. V. K. Patnana, R. P. Bharti and R. P. Chhabra, *Int. J. Heat Mass Transfer.*, **53**, 4152 (2010).
30. A. T. Srinivas, R. P. Bharti and R. P. Chhabra, *Ind. Eng. Chem. Res.*, **48**, 9735 (2009).

31. R. P. Bharti, R. P. Chhabra and V. Eswaran, *Chem. Eng. Sci.*, **62**, 4729 (2007).
32. R. P. Bharti, R. P. Chhabra and V. Eswaran, *Ind. Eng. Chem. Res.*, **46**, 3820 (2007).
33. M. K. Rao, A. K. Sahu and R. P. Chhabra, *Polym. Eng. Sci.*, **51**, 2044 (2011).
34. S. Bijjam and A. K. Dhiman, *Chem. Eng. Commun.*, **199**, 767 (2012).
35. T. Igarashi, *Int. J. Heat Mass Transfer.*, **30**, 893 (1987).
36. G. R. Ahmed and M. M. Yovanovich, *Trans. ASME J. Heat Transfer.*, **119**, 70 (1997).
37. A. K. Saha, K. Muralidhar and G. Biswas, *Exp. Fluids*, **29**, 553 (2000).
38. S. K. Singh, P. K. Panigrahi and K. Murlidhar, *Exp. Fluids*, **43**, 101 (2007).
39. N. E. Sabiri, R. P. Chhabra, J. Comiti and A. Montillet, *Exp. Therm. Fluid Sci.*, **39**, 167 (2012).
40. R. W. Davis, E. F. Moore and L. P. Purtell, *Phys. Fluids*, **27**, 46 (1984).
41. K. Suzuki and H. Suzuki, *Unsteady heat transfer in a channel obstructed by an immersed body*, *Annu. Rev. Heat Transfer*, C. L. Tien (Ed.), Begell House, New York, **5**, 177 (1994).
42. P. M. Coelho and F. T. Pinho, *J. Non-Newtonian Fluid Mech.*, **110**, 143 (2003).
43. P. M. Coelho and F. T. Pinho, *J. Non-Newtonian Fluid Mech.*, **110**, 177 (2003).
44. P. M. Coelho and F. T. Pinho, *J. Non-Newtonian Fluid Mech.*, **121**, 55 (2004).
45. A. K. Dhiman, *Flow over and heat transfer to power-law fluids across a square cylinder in steady regime: A numerical study*, Ph.D. Thesis, Indian Institute of Technology Kanpur, India (2006).
46. J. F. Thompson, Z. U. A. Warsi and C. W. Mastin, *Numerical grid generation: Foundations and applications*, Elsevier Science, New York, 305 (1985).
47. A. Sharma and V. Eswaran, *A finite volume method*, in K. Muralidhar and T. Sundararajan (Eds.), *Computational Fluid Flow and Heat Transfer*, Narosa Publishing House, New Delhi, 445 (2003).
48. C. M. Rhie and W. L. Chow, *AIAA J.*, **21**, 1525 (1983).
49. A. K. Dhiman, N. Sharma and S. Kumar, *Brazilian J. Chem. Eng.*, **29**, 253 (2012).
50. U. Ghia, K. N. Ghia and C. T. Shin, *J. Comput. Phys.*, **48**, 387 (1982).
51. A. Dhiman, N. Sharma and S. Kumar, *Int. J. Sustainable Energy*, http://dx.doi.org/10.1080/14786451.2013.764878 (2013).
52. G. Gandikota, S. Amiroudine, D. Chatterjee and G. Biswas, *Numer. Heat Transfer. Part A*, **58**, 385 (2010).
53. D. Chatterjee, *Numer. Heat Transfer. Part A*, **61**, 800 (2012).
54. D. Chatterjee and B. Mondal, *Comput. Therm. Sci.*, **4**, 23 (2012).
55. P. J. Roache, *Verication and validation in computational science and engineering*, Hermosa Publishers, Albuquerque, New Mexico (1998).